Carnot batteries for integrated heat and power management in residential applications: a techno-economic analysis

Antoine Laterre[a,c,*], Guido Francesco Frate[b], Vincent Lemort[c], Francesco Contino[a]

[a] *Institute of Mechanics, Materials and Civil Engineering (iMMC), Université catholique de Louvain (UCLouvain), Place du Levant, 2, Louvain-la-Neuve, 1348, Belgium*
[b] *Department of Energy, Systems, Territory and Constructions Engineering, University of Pisa, Largo Lucio Lazzarino, Pisa, 56122, Italy*
[c] *Thermodynamics Laboratory, University of Liège (ULiège), Allée de la Découverte 17, Liège, 4000, Belgium*

Abstract

The growing use of photovoltaic (PV) energy in residential systems presents challenges, notably managing daily and seasonal intermittency. To limit curtailment and maximise self-consumption, decentralised flexibility options are crucial. In this context, Carnot batteries, which combine a heat pump, thermal energy storage, and a heat engine, show promise for integrated heat and power management alongside PV production. However, the economic model (investment costs, electricity pricing system) and control strategy (heat/electricity discharge, seasonal impacts) needed to achieve maximum cost-effectiveness have not yet been identified. This study therefore explores the integration of a Carnot battery in a housing development of 20 dwellings equipped with PV systems. Using a quadratically constrained linear programming model, the designs and operations that minimise the annualised energy cost are identified across different ranges of investment costs. The impact of climatic conditions is assessed by comparing results from Pisa and Brussels. Our findings indicate that, except in scenarios with prohibitively high costs, incorporating a heat engine alongside a heat pump and thermal energy storage is the most cost-effective solution. Parametric analyses reveal that zero feed-in tariffs promote Carnot battery deployment, while non-zero tariffs significantly reduce the installed capacity. Additionally, dynamic (or variable) tariffs

*Corresponding author.
Email address: antoine.laterre@uclouvain.com (Antoine Laterre)

generally do not reduce energy costs but do increase the Carnot battery capacity, in order to take advantage of the energy arbitrage mechanism. In conclusion, when heat pumps and thermal storage are necessary to meet heating demand, adding a heat engine to address electricity needs is financially effective. This paves the way for further advancements in residential energy management using Carnot batteries. Future work should confirm and refine these results with more precise models, incorporating non-linearities such as start-up and part-load operations.

Keywords:
Carnot Battery, Residential Photovoltaics, Sector Coupling, Techno-Economic Analysis, Design Optimisation, Optimal Scheduling, Quadratically Constrained Linear Programming

---

1. Introduction

With the transition to renewable energies, energy systems are shifting from a vertical structure to an increasingly decentralised and distributed architecture. The growing development of residential photovoltaics is a perfect illustration. However, this morphological change poses a series of challenges, not least the local management of the intermittency and non-pilotability of renewable energies. In the case of residential photovoltaics, for example, peak production is reached at midday, while peak energy demand (heat and electricity) occurs in the morning and evening. Also, seasonally, peak production occurs in spring/summer period, while peak demand occurs in autumn/winter period (in northern hemisphere) [1].

This mismatch between production and demand leads at certain times to a net local excess of power, which is becoming increasingly difficult for residential distribution grids to absorb [2]. These are constrained by the fact that other prosumers are also facing overproduction, and that reversing the power flows between the distribution and transmission grids is not always possible (technological constraints linked to handling bidirectional flows, grid congestion, etc.) [2]. Alongside work on the elasticity of demand, the need for decentralised and cost-effective flexibility options is becoming ever more pressing, without which this precious renewable energy will have to be curtailed [3].

Nomenclature

Greek and Latin symbols		disch	discharge
ΔT	temperature difference, °C	dless	dimensionless
$\dot{Q}$	thermal power flow, kW_{th}	elec	electricity
η	efficiency, %	el	electric
Ψ^{Lorenz}	fraction of Lorenz efficiency, -	ext	external
τ	annualisation factor, %	inj	injected (fed-in)
CV	coefficient of variation, %	nom	nominal capacity
E	electricity costs, €	p	peak
E	energy, kWh	th	thermal
I	investment costs, €	*Symbols*	
L	self-discharge losses, %/24 h	AEC	annualised energy cost
M	maintenance costs, €	CAPEX	capital expenditures, €
P	electric power flow, kW_{el}	CB	Carnot battery
p	price, %	COP	coefficient of performance, -
r	discount rate, %	HE	heat engine
T	temperature, °C	HP	heat pump
Sub- and superscripts		LCOS	levelised cost of storage
abs	absorbed (retailed)	PV	photovoltaic system
ch	charge	SOC	state of charge, %
crt	curtailed	TES	thermal energy storage

In residential energy systems, although the renewable production is mostly in the form of electricity (photovoltaics is usually preferred to solar thermal due to its versatility and high exergy density), the majority of the energy demand is in the form of heat (space heating, domestic hot water). From this perspective, heat pumps appear to be an effective way of combining these two vectors [4, 5]. Furthermore, the addition of domestic thermal energy storage can help to bridge the gap between production and demand, at least on a daily basis [5–7]. However, as the demand for heat decreases during the spring/summer season, electricity storage options must also be installed to increase self-consumption and limit curtailment [4–7].

1.1. Carnot batteries for heat and power management

Among the various flexibility options, Carnot batteries could prove very useful in residential applications [8–11]. This concept converts surplus electricity into heat and charges it into a thermal energy storage. Then, when electricity is needed, it can be generated by a heat engine powered by the thermal storage. At small scale (e.g. residential), the concept would use vapor compression heat pumps for charging and organic Rankine cycles for discharging [10, 12]. On a larger scale (e.g. industrial, transmission grid), the concept is more often implemented with closed Brayton cycles [10, 13].

As well as storing electricity, the Carnot batteries strength lies in the way they combine heat and electricity. As illustrated in Fig. 1, a heat source of a higher grade than the heat sink of the heat engine can be used to boost the performance of the heat pump (waste heat, geothermal, solar thermal, waste water, etc.). Also, the energy stored in the thermal energy storage can directly be discharged in the form of heat. This multi-energy capability is of particular interest in residential applications to cover both thermal and electrical demands [8].

For future decentralised renewable energy systems, studies have already shown that installing photovoltaic systems coupled with heat pumps and thermal storages is an effective way of reducing greenhouse gas emissions, while reducing energy bills and increasing resilience to fluctuations in market prices [4, 6, 7]. From this perspective, the simple addition

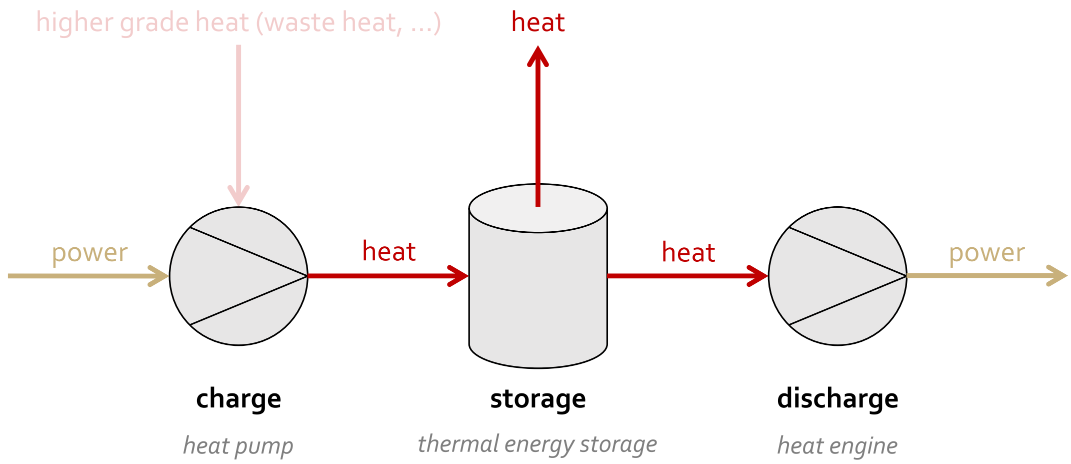

Figure 1: Schematic diagram of a Carnot battery coupling heat and electricity.

of a heat engine would make it possible to provide electricity storage, which would make it possible to limit curtailment in summer when demand for heat is at its lowest. Or even better than adding a heat engine: using a reversible heat pump/organic Rankine cycle, which would reduce investment costs [14–17]. The question is under what conditions (investment costs, electricity pricing system, etc.) would this make economic sense?

Techno-economic studies on Carnot batteries utilising vapor compression heat pumps and organic Rankine cycles (known as Rankine-based Carnot batteries) started to emerge in 2020-2021 [18, 19]. Some cover systems coupling the heat and electricity vectors, while others focus exclusively on power-to-power applications, generally at grid level [20–22]. In the following literature review, only Carnot batteries integrating heat and electricity are covered. This review is also reported in Table 1.

Two main approaches can be distinguished in the literature to assess the techno-economic performance of Carnot batteries. The first is generally aimed at determining the levelised cost of storage (LCOS) of the technology, assuming ideal operations (i.e. 365 complete charge-discharge cycles over the year). To do this, the cost of each component is evaluated on the basis of empirical correlations. An electricity purchase and resale price is also assumed. For example, Hu et al. [19] looked at the efficiency and the LCOS of Carnot batteries using

Table 1: Review of techno-economic studies on Carnot batteries with coupling between thermal and electrical vectors. PCM stands for Phase Change Material. MILP is for Mixed Integer Linear Programming.

Reference	**Case study**	**Heat source**	**Storage**	**Discharge**	**Resolution**	**Operations**
Frate et al. [18], 2020	parametric analysis	unspecified (60-80°C)	two water tanks (80-95°C)	electrical	n.a.	n.a.
Hu et al. [19], 2021	parametric analysis	waste heat, solar thermal, geothermal, district heat. (55-85°C)	two water tanks (85-100°C)	electrical	ideal cyclic (365 cycles)	n.a.
Fan and Xi [23, 24], 2022	parametric analysis	waste heat (80°C)	two water tanks (90-130°C)	electrical	ideal cyclic (365 cycles)	n.a.
Zhang et al. [25], 2022	parametric analysis	waste heat (85°C)	two water tanks (90-120°C)	electrical	ideal cyclic (365 cycles)	n.a.
Niu et al. [26], 2023	parametric analysis	unspecified + solar thermal (60°C)	two water tanks (90-130°C)	electrical	two typical days (1-hour steps)	rule based
Yu et al. [27], 2023	parametric analysis	unspecified (60-95°C)	two water tanks (90-125°C)	electrical	ideal cyclic (365 cycles)	n.a.
Su et al. [28], 2023	parametric analysis	geothermal (140°C)	single water tank (150°C)	electrical	ideal cyclic (7000h operations)	n.a.
Tassenoy et al. [29], 2022	office building with PV	data centre cooling (50°C)	sensible heat (100°C)	electrical	typical year (15-min steps)	rule based
Scharrer et al. [30], 2022	residential district with PV	unspecified (70°C)	single water tank (90-120°C)	electrical	typical year (1-min steps)	rule based
Datas et al. [11], 2019	residential building with PV	n.a. (Joule heating)	single water tank (70-130°C) + PCM (1200°C)	electrical, thermal	typical year (1-hour steps)	rule based
Frate et al. [9], 2023	multi-energy district with PV	solar thermal (60-90°C)	hot PCM (70-100°C), cold PCM (7°C)	electrical, thermal, cooling	typical year (1-hour steps)	optimised (MILP)
Poletto et al. [31], 2024	office building with PV	waste heat, district heat. (60°C)	single water tank (65-100°C)	electrical, thermal	typical year (15-min steps)	rule based (optimised)
Laterre et al. [32], 2024	data centre with PV	data centre cooling (24-60°C)	two water tanks (100-150°C)	electrical	typical year (1-hour steps)	rule based

heat pumps combined with different heat sources (waste heat, solar thermal, geothermal and district heating) at various temperatures (55, 65, 75 and 85°C). The thermal energy is stored as sensible heat in two water reservoirs. It is then discharged in the form of electricity via an organic Rankine cycle. They have shown that once optimised, efficiency and LCOS are conflicting objectives. Frate et al. [18] extended this result by showing that for different power ranges, source temperatures (60, 70 and 80°C) and charging times, the purchased equipment cost is always in conflict with the efficiency. Fan and Xi [23, 24], and Zhang et al. [25] compared the performance of four different Carnot battery topologies based on vapour compression heat pumps and organic Rankine cycles, with and without internal recuperators. Considering some 80°C waste heat as heat source, they confirmed that storage efficiency and LCOS are strictly conflicting. In addition, they demonstrated that despite requiring a higher investment cost, cycles with internal recuperators give a higher efficiency and a lower LCOS. Niu et al. [26] looked at a Carnot battery supplemented by solar thermal collectors connected directly to the thermal storage. Using two typical days (winter and summer solstices), they also demonstrated that the storage efficiency and LCOS are improved in the case of cycles with internal recuperators. Yu et al. [27] also looked at the LCOS and efficiency of Carnot batteries with different topologies using heat sources ranging from 60 to 95°C. They came to the same conclusions as the aforementioned studies. Finally, Su et al. [28] looked at geothermal-assisted Carnot batteries and concluded that despite requiring a higher investment cost, the use of a geothermal source increases the profitability of the system. In general, all these studies conclude that despite high investment costs, Carnot batteries show great techno-economic potential and could be competitive with other storage technologies such as batteries, pumped-hydro or liquid and compressed air (but without specifying the costs used for comparison). It should be noted, however, that they have not characterised the full potential of Carnot batteries because only the electrical discharge was exploited, and not the thermal discharge.

The second approach used in techno-economic studies of Carnot batteries for heat and power coupling is generally more conservative, as it assumes more realistic operating cycles.

It is based on case studies using real (or at least realistic) time series as boundary conditions. In this way, fluctuations in renewable energy production, energy demand levels and possibly electricity prices can be captured over the 8760 hours of typical years. In these models, the operations of the Carnot battery are usually simulated using an energy management system guided by predefined rules, such as "if excess renewable production then charge" and "if under-production then discharge". Under these assumptions, the studies often turn out to be much less optimistic than those cited above. For example, Tassenoy et al. [29] looked at the integration of a Carnot battery recycling waste heat from a data centre to provide electricity storage to an office building. Coupled with a photovoltaic system, the optimisation objective was to maximise the net present value. The authors demonstrated that without a subsidy/tax mechanism, it was not possible to achieve financial feasibility. Scharrer et al. [30] studied the implementation of a Carnot battery based on a reversible heat pump/organic Rankine cycle in a residential area. The nature of the 70°C heat source was unspecified, but different costs were investigated for it. Only electrical discharge was considered (no thermal discharge to cover the heat demand of the dwellings). They concluded that, with a storage efficiency above 50 %, assuming high electricity prices and in the event of a non-zero feed-in tariff, only the case where the heat supplied to the heat pump was available for free made it possible to achieve economic feasibility. However, the Carnot battery generated limited savings (maximum 180€ per year per dwelling) and gave rise to payback periods of 13 years. Datas et al. [11] also considered the integration of very high temperature (>> 500°C) joule heating based Carnot batteries in residential sector. The low-temperature heat generated by the heat engine during discharge could be stored in a buffer reservoir to meet the heating needs (a fuel boiler was available as backup). For a detached house with a PV system, they showed that electricity savings of 70 % and fuel savings of 20 % could be reached, but only under (unrealistically) favourable conditions (heat engine cost of 1000 €/kW_{el} and heat engine efficiency of 40 %). For more conservative assumptions (2000 €/kW_{el} and 20 % efficiency), no more storage capacity was deployed. Frate et al. [9] looked at the integration of Carnot batteries in multi-energy districts based on photovoltaic and solar thermal, and with cooling, low temperature and high temperature thermal networks. They also considered the gas and electrical grids as backups. For a given design, they optimised the system's operations (i.e. no rule based strategy) in order to minimise its total annualised cost (investment and operations). They have shown that, although they are currently financially unfeasible, Carnot batteries offer a greater reduction in greenhouse gas emissions than lithium-ion batteries. For their part, Poletto et al. [31] studied the optimum control strategy for Carnot batteries connected to district heating networks or recovering waste heat, and integrated into office buildings. The system made it possible to downsize the district heating substation by acting as a buffer to cope with the morning peak in thermal demand, and to shift the production of photovoltaic energy. As the machine was based on a reversible heat pump/organic Rankine cycle, electrical discharge was also permitted. Results showed that most of the profit came from the thermal discharge and downsizing the substation, and to a very lesser extent from the electrical discharge. It was also shown that the case where the heat pump drew its source from the heating network did not make it possible to reach financial feasibility. Finally, Laterre et al. [32] looked at the integration of Carnot batteries in data centres. Coupled with a photovoltaic system, the aim was to increase the data centres energy self-sufficiency while recovering the waste heat. The results showed that Carnot batteries using ambient air as heat source instead of waste heat provided better techno-economic performance, because the amount of available waste heat was limited (i.e. it was equal to the data centre electrical consumption), which constrained the amount of electricity that could be stored.

Apart from three studies [9, 11, 31], all the above cited works only considered electrical discharge for the Carnot battery. Specifically, apart from Frate et al. [9] who concluded that it was not economically viable, none have investigated the use of Carnot batteries as proper flexibility options for heat and power management. Finally, none of them simultaneously optimised the system design (i.e. components capacity) and the power dispatch (equivalent to the energy management strategy). But this approach would precisely make it possible to identify the optimum conditions for maximising the profitability of Carnot batteries.

1.2. Aims of this study and work novelty

The aim of this work is therefore to identify the economic conditions that will enable Carnot batteries to be used as flexibility options for heat and electricity management in residential applications. The case study will focus on a housing development of 20 dwellings, so that an hourly resolution is sufficient to capture the overall fluctuation in demand (which may be more dynamic at the level of individual dwellings).

As preliminary studies involving fixed designs generally tend to show that financial profitability is not good [9, 31], the design and operations of the energy system will be simultaneously optimised to minimise the annualised energy cost and guarantee optimum performance. This optimisation model will be implemented using quadratically constrained linear programming. Also, as the technology readiness level (TRL) of Carnot batteries is relatively low, their retail price is still uncertain. In order to capture this reality, this study will be carried out in the form of a parametric analysis. The costs of the three main components of the Carnot battery will be varied (i.e. heat pump, thermal storage and heat engine). The cost ranges considered represent those currently proposed in the literature. For each combination of these costs, the optimal design for the Carnot battery will then be identified. The aim is to understand at what investment costs the Carnot battery, combined with the photovoltaic system, would minimise the annualised energy cost. In other words, when does it become more cost-effective than a system based solely on photovoltaics and/or thermal storage?

To illustrate the impact of climatic conditions on the system performance (energy demand, photovoltaic production), two locations will be considered. The effect of the electricity pricing model will also be evaluated by considering fixed and dynamic retail tariffs, and by considering zero and non-zero feed-in tariffs. A sensitivity analysis to technical and operational parameters will also be conducted to identify the uncertainty to which the annualised energy cost is most sensitive. A detailed operational analysis will also be carried out to identify and understand how the Carnot battery should be operated in order to deliver optimum performance.

Finally, a discussion will allow to extrapolate the results obtained using this model in order to identify how residential Carnot batteries could develop in the real world. This discussion will also challenge the assumptions made when formulating the model.

2. Model and methods

The energy system in which the Carnot battery is integrated is first introduced. After that, the economic model and cost correlations are explained. Then, the optimisation model is detailed. Finally, the uncertainty propagation method for the sensitivity analysis is briefly described.

2.1. Carnot batteries in residential application

The Carnot battery considered in this work is part of a housing development of 20 dwellings, as shown in Fig. 2. This consists of a high temperature heat pump, a sensible

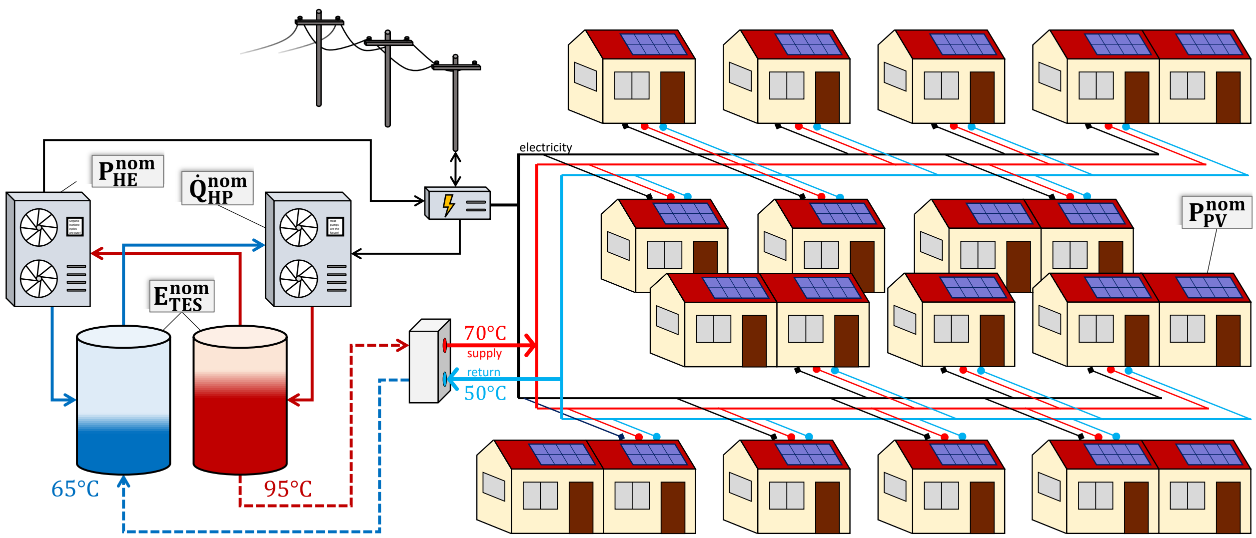

Figure 2: Schematic representation of the energy system of the housing development. P_{PV}^{nom} [kW_p] is the nominal capacity of the PV system, $\dot{Q}_{HP}^{nom}$ [kW_{th}] the nominal heat pump capacity, E_{TES}^{nom} [kWh_{th}] the nominal storage capacity and P_{HE}^{nom} [kW_{el}] the nominal heat engine capacity. Illustration inspired from [30].

heat thermal energy storage (hot water) and a heat engine. The heat pump uses outside air as heat source (air-source heat pump). The heat engine, which is implemented as an organic Rankine cycle, also uses outside air as heat sink.

In this energy system, the heat pump can be powered by the photovoltaic system and by the distribution grid. It produces heat at 95°C (return at 65°C), which can be consumed directly by the dwellings via a district heating network (supply 70°C, return 50°C) or charged into the thermal energy storage. The energy consumption associated with the start-up procedure of the system is discussed in the heat pump model in Section 2.3.2. As sensible heat needs a temperature gradient to be accumulated, the choice of 95°C and 65°C as temperatures is the result of a compromise between storage density (and therefore volume and cost), the constraint of using non-pressurised reservoirs (cost reduction), and operating the heat engine with sufficient efficiency so that the power-to-power efficiency of the Carnot battery is not too low [33, 34]. This choice is further elaborated in the discussion (Section 4). For the considered two-tanks storage, the energy density is defined as

$$\rho_{\mathrm{TES}} = \frac{\int_{\mathrm{T_{TES}^{lt}}}^{\mathrm{T_{TES}^{ht}}} \mathrm{c_p^{H2O}(T)\,dT}}{3.6\mathrm{e}{+}6 \cdot \left(\mathrm{v_{H2O}^{lt}} + \mathrm{v_{H2O}^{ht}}\right)} \left[\frac{\mathrm{kWh_{th}}}{\mathrm{m^3}}\right] , \tag{1}$$

with $\mathrm{c_p^{H2O}}$ the specific heat capacity and $\mathrm{v_{H2O}}$ the specific volume of water. $\mathrm{T_{TES}^{lt}}$ and $\mathrm{T_{TES}^{ht}}$ are the cold and hot tank temperatures respectively. The total storage volume (combined cold and hot tanks) is therefore defined as

$$\mathrm{V_{TES}} = \frac{\mathrm{E_{TES}}}{\rho_{\mathrm{TES}}} \left[\mathrm{m^3}\right] , \tag{2}$$

with $\mathrm{E_{TES}}$ [$\mathrm{kWh_{th}}$] the storage capacity.

The performance parameters representing the components of the energy system are shown in Table 3. They will be discussed further in the description of the optimisation model (Section 2.3).

Time series with hourly resolution were used to represent the climate and demand data of the case study, as depicted in Fig. 3. These were generated using the nPro 2.0 software [35] to represent a development of 20 dwellings. Each has a floor area of 150 $\mathrm{m^2}$. Pisa was selected as reference location for this study. However, in order to extend the results and assess the impact of climatic conditions on the design of the energy system, Section 3.5 also

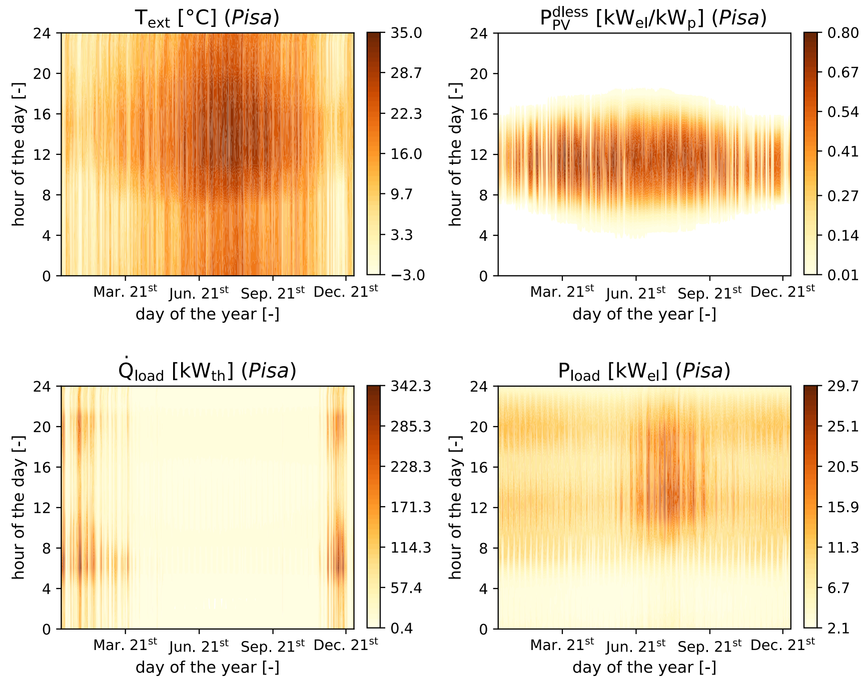

Figure 3: Temporal heatmaps representing the climate and demand profiles for Pisa. The the days of the year are plotted along the x-axis, and hours of the day are plotted along the y-axis. P_{load} and $\dot{Q}_{load}$ are the total electrical and thermal loads. T_{ext} is the external temperature and P_{PV}^{dless} is the dimensionless photovoltaic production per installed capacity.

compares these to the case of Brussels (the corresponding boundary conditions are provided in Fig. A.1 in Appendix A).

The specific heating requirements are 69 kWh/m^2/year and the domestic hot water demand is 21 kWh/m^2/year. The electricity demand is 20 kWh/m^2/year. Finally, the specific cooling requirements are 36 kWh/m^2/year. Cooling is provided by decentralised air-cooled chillers. Assuming that the units have a Carnot efficiency of 45 %, the corresponding specific electricity consumption is 4.1 kWh/m^2/year. This additional electricity consumption must be added to the specific electricity demand of 20 kWh/m^2/year. These values are the default values for new build buildings in nPro 2.0 [35]. It should be noted that the thermal demand dominates the global energy consumption. The impact of reducing this demand (thanks to building insulation, etc.) will be discussed in Section 4.

In Fig. 3, $\dot{Q}_{load}$ represents the total thermal load (space heating and domestic hot water) and P_{load} the electrical load (plug loads and cooling). T_{ext} is the external temperature, and P_{PV}^{dless} is the dimensionless photovoltaic production per installed capacity (accounting simultaneously for irradiance and inverter losses, as explained in the model description in Section 2.3.4).

Fig. 3 shows that the demand for heat is lowest in spring and summer when the photovoltaic system produces the most. As suggested by previous analyses [9, 31], we can therefore expect more electricity to be stored at this time of year than in autumn and winter. In addition, energy demand peaks are in the morning and evening, whereas the photovoltaic system mainly produces in the middle of the day. This clearly illustrates the need for daily buffer storage, which could be provided by the Carnot battery.

2.2. Economic model

2.2.1. Annualised energy cost

The aim of this work is to understand the role that the Carnot battery can play in a residential energy system as a function of the underlying investment costs. In other words, at what cost does it become more attractive to store photovoltaic energy rather than buy electricity from the grid? To answer this question, different sets of investment costs were considered (see Table 2) and the annualised energy cost (AEC) was chosen as the objective function to be minimised. Such parameter is defined as

$$\mathrm{AEC} = \tau \mathrm{I} + \mathrm{M} + \mathrm{E} \ , \tag{3}$$

where I is the investment cost, M the maintenance cost, E the electricity cost, and τ the annualisation factor (or capital recovery factor) [36]. The latter is defined as

$$\tau = \frac{\mathrm{r}(1+\mathrm{r})^{\mathrm{LT}}}{(1+\mathrm{r})^{\mathrm{LT}}-1} \ , \tag{4}$$

with LT the project lifetime and r the discount rate. The corresponding values are reported in Table 2. Note that the discount rate of 7 % is relatively conservative given the maturity of the technologies under consideration (i.e. photovoltaic system, heat pump, water thermal storage). As a result, it will tend to limit the share of investments in the annualised energy cost and favour variable costs (i.e. grid electricity consumption).

Table 2: Economic parameters of the model.

Parameter	**Symbol**	**Value/Definition**	**Unit**	**Reference**
Investment cost	I	$CAPEX_{PV+HP+TES+HE}$	€	n.a.
PV investment cost	$CAPEX_{PV}$	1000	€/kW_p	[37]
HP investment cost	$CAPEX_{HP}$	200 - 1200	€/kW_{th}	[6, 9, 38]
TES investment cost	$CAPEX_{TES}$	20 - 40	€/kWh_{th}	[9, 29, 30]
HE investment cost	$CAPEX_{HE}$	400 - 6000	€/kW_{el}	[9, 29, 39, 40]
Lifetime	LT	20	years	[9, 19, 23, 29]
Discount rate	r	7.0	%	[9, 19, 23, 29]
Annualisation factor	τ	9.4	%	Eq. 4
Maintenance cost	M	$0.02 \cdot I$	€	[9, 19, 23, 29]
Electricity cost	E	$p_{elec}^{abs} E_{grid}^{abs} - p_{elec}^{inj} E_{grid}^{inj}$	€	n.a.
Retail tariff	p_{elec}^{abs}	0.30	€/kWh_{el}	[30, 41]
Feed-in tariff	p_{elec}^{inj}	0.00	€/kWh_{el}	n.a.

As there is little information at this stage on the maintenance costs of Carnot batteries, these are defined as a fraction of the total investment cost. This simplifying approach is generally used in techno-economic studies of Carnot batteries [9, 19, 23, 27, 29]. A value of 2 % is chosen here to represent the ranges from 1.5 % [19, 23, 27, 29] to 3 % [9] encountered in the literature.

2.2.2. Electricity pricing model

The electricity cost E is represented as the difference between the purchasing cost (product of retail tariff and absorbed electricity) and the injection gain (product of feed-in tariff and injected electricity). By default, a constant electricity price p_{elec} of 0.30 €/kWh_{el} is considered. Also note that the default feed-in tariff is zero, but a parametric analysis is carried out in Section 3.3.1.

As mentioned in the introduction, a parametric analysis is also carried out to study the impact of dynamic (or "variable") retail tariffs in Section 3.3.2. More specifically, the aim is to identify the level of fluctuation at which the Carnot battery can reduce the annualised energy cost. The electricity price model that was used in this work is depicted in Fig. 4 for three different levels of fluctuation. This model was constructed as

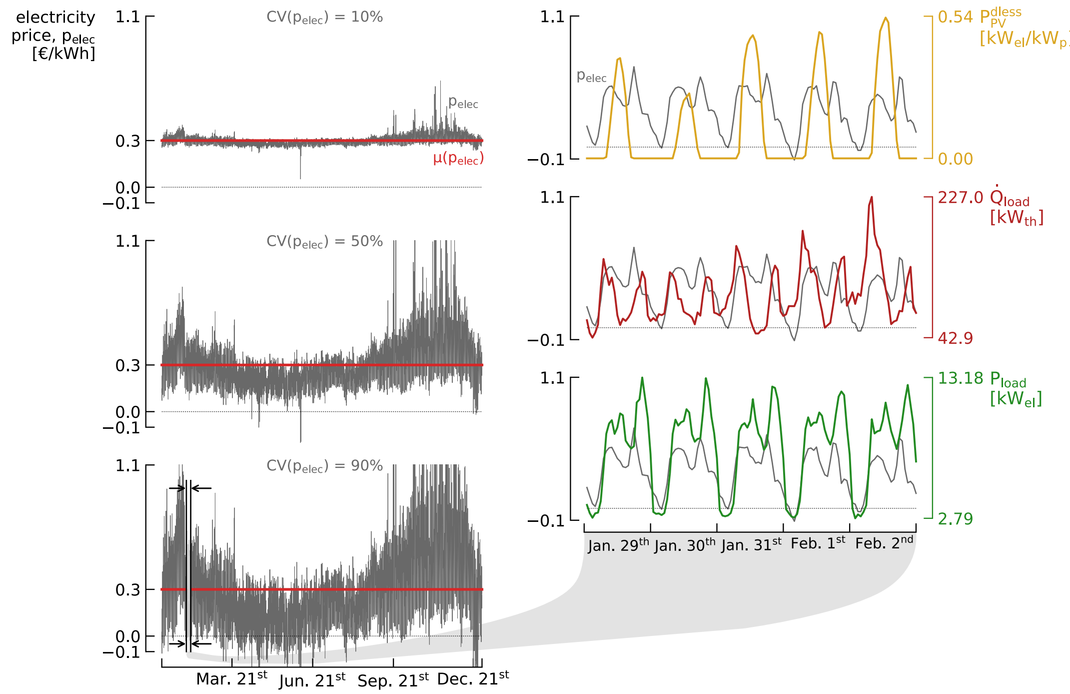

Figure 4: Model for electricity price $p_{elec}[t]$ with $CV(p_{elec}) = \sigma(p_{elec})/\mu(p_{elec})$ = 10, 50 and 90 %. Values are cropped to -0.1 - 1.1 for clarity but can go below and above. P_{PV}^{dless}, $\dot{Q}_{load}$ and P_{load} are reported for five representative days in Pisa to illustrate the correlation between energy demand and electricity price on a daily basis. Seasonal trends are also visible.

$$p_{elec}[t] = \alpha \cdot p_{day-ahead}[t] + \beta \ , \tag{5}$$

with α and β subject to

$$\mu(p_{elec}) = \mu(\alpha \cdot p_{day-ahead}[t] + \beta) = 0.30 \text{ €/kWh}_{el} \quad , \tag{6}$$

$$CV(p_{elec}) = \frac{\mu(\alpha \cdot p_{day-ahead}[t] + \beta)}{\sigma(\alpha \cdot p_{day-ahead}[t] + \beta)} \ , \tag{7}$$

with μ the mean, σ the standard deviation and CV the coefficient of variation. In Eq. 5, $p_{day-ahead}[t]$ is the day-ahead spot market price for delivery at hour t. The constraint on the average electricity price in Eq. 6 is employed so as to make a sound comparison with the fixed retail tariff scenarios. The value of $p_{day-ahead}$ was taken as the average of historical values between 2015 and 2020 for the Belgian day-ahead prices (before COVID-19 pandemic and global 2021-2023 energy crisis). Data was retrieved using the ENTSO-E Transparency Platform [42].

2.3. Optimisation model

The energy system model must optimise the design (i.e., nominal capacities) and power flow schedule for each of the 8760 hours of the year so as to minimise the annualised energy cost. This has been implemented in `Python` using the `pyomo` package [43] with a quadratically constrained linear formulation of the problem. `Gurobi` [44] was used as a solver. This model is described below. All associated parameters are listed in the Table 3.

Table 3: Technical parameters of the model.

Parameter	Symbol	Value	Unit
HP source temperature	T_{HP}^{source}	T_{ext}	°C
HP source temperature glide	ΔT_{HP}^{source}	5	K
HP fraction of Lorenz efficiency	Ψ_{HP}^{Lorenz}	0.50	-
HE sink temperature	T_{HE}^{sink}	T_{ext}	°C
HE sink temperature glide	ΔT_{HE}^{sink}	5	K
HE fraction of Lorenz efficiency	Ψ_{HE}^{Lorenz}	0.45	-
TES high temperature	T_{TES}^{ht}	95	°C
TES low temperature	T_{TES}^{lt}	65	°C
TES energy density	ρ_{TES}	17	kWh_{th}/m^3
TES self-discharge	L_{TES}	5	%/24 h

2.3.1. Global model structure

The model contains the four design variables (i.e. P_{PV}^{nom}, $\dot{Q}_{HP}^{nom}$, E_{TES}^{nom} and P_{HE}^{nom}) and the power flow variables (one for each of the 8760 hours of the year). These flow variables are:

- $P_{grid}^{abs}[t]$, the electrical power absorbed from the grid;

- $P_{grid}^{inj}[t]$, the electrical power fed into the grid;
- $\dot{Q}_{HP}[t]$, the thermal power produced by the heat pump;
- $P_{HP}[t]$, the electrical power absorbed by the heat pump;
- $\dot{Q}_{TES}^{ch}[t]$, the charging thermal power for the thermal energy storage;
- $\dot{Q}_{TES}^{disch}[t]$, the discharging thermal power for the thermal energy storage;
- $SOC_{TES}[t]$, the state of charge of the the thermal energy storage;
- $\dot{Q}_{HE}[t]$, the thermal power absorbed by the heat engine;
- $P_{HE}[t]$, the electrical power produced by the heat engine;
- $P_{PV}^{crt}[t]$, the curtailed photovoltaic power.

Under steady state assumption, power conservation is applied to each component and each node (electrical and thermal) of the energy system via equality constraints. Power flows are contained between zero and the nominal capacity of each component using inequality constraints. These equality and inequality constraints for each component are detailed below. The only quadratic constraint is used to avoid bidirectional exchanges with the grid, as detailed below.

The optimisation is based on the assumption of perfect foresight. This means that climatic conditions and demand data are perfectly known in advance. The impact and plausibility of this assumption will be further challenged in Section 4.

2.3.2. Heat pump and heat engine

Due to the linear formulation of the problem, no thermodynamic model could be used to simulate the heat pump and the heat engine. These are therefore represented by a black-box model, which is based on the theoretical Lorenz cycle (more appropriate than the Carnot cycle for representing applications with large temperature glides [45–47]). Assuming a constant fraction Ψ^{Lorenz} of the Lorenz efficiency, which is analogous to a second law efficiency, this model evaluates the variations in $\mathrm{COP_{HP}}$ and η_{HE} due to fluctuations in source and sink temperatures. Although it is less accurate than more advanced methods, its light linear formulation makes it popular for energy planning problems [46, 48, 49].

For the heat pump, the Lorenz model connects $\dot{\mathrm{Q}}_{\mathrm{HP}}[\mathrm{t}]$ and $\mathrm{P_{HP}}[\mathrm{t}]$ under steady state assumption with the following power balance:

$$\begin{aligned}\dot{\mathrm{Q}}_{\mathrm{HP}}[\mathrm{t}] &= \mathrm{P_{HP}}[\mathrm{t}] \cdot \mathrm{COP_{HP}}[\mathrm{t}] && (8)\\ &= \mathrm{P_{HP}}[\mathrm{t}] \cdot \Psi_{\mathrm{HP}}^{\mathrm{Lorenz}} \cdot \mathrm{COP}_{\mathrm{HP}}^{\mathrm{Lorenz}}[\mathrm{t}] && (9)\\ &= \mathrm{P_{HP}}[\mathrm{t}] \cdot \Psi_{\mathrm{HP}}^{\mathrm{Lorenz}} \cdot \frac{\overline{\mathrm{T}}_{\mathrm{H}}}{\overline{\mathrm{T}}_{\mathrm{H}} - \overline{\mathrm{T}}_{\mathrm{C}}[\mathrm{t}]}\ . && (10)\end{aligned}$$

$\dot{\mathrm{Q}}_{\mathrm{HP}}[\mathrm{t}]$ and $\mathrm{P_{HP}}[\mathrm{t}]$ are the thermal and electrical power at instant t, respectively. $\overline{\mathrm{T}}_{\mathrm{C}}[\mathrm{t}]$ and $\overline{\mathrm{T}}_{\mathrm{H}}$ are the mean source and sink temperatures, defined as

$$\overline{\mathrm{T}}_{\mathrm{C}}[\mathrm{t}] = \frac{\mathrm{T}_{\mathrm{HP}}^{\mathrm{source}}[\mathrm{t}] - (\mathrm{T}_{\mathrm{HP}}^{\mathrm{source}}[\mathrm{t}] - \Delta \mathrm{T}_{\mathrm{HP}}^{\mathrm{source}})}{\ln\left(\frac{\mathrm{T}_{\mathrm{HP}}^{\mathrm{source}}[\mathrm{t}]}{\mathrm{T}_{\mathrm{HP}}^{\mathrm{source}}[\mathrm{t}] - \Delta \mathrm{T}_{\mathrm{HP}}^{\mathrm{source}}}\right)}\ ,\ \ \overline{\mathrm{T}}_{\mathrm{H}} = \frac{\mathrm{T}_{\mathrm{TES}}^{\mathrm{ht}} - \mathrm{T}_{\mathrm{TES}}^{\mathrm{lt}}}{\ln\left(\frac{\mathrm{T}_{\mathrm{TES}}^{\mathrm{ht}}}{\mathrm{T}_{\mathrm{TES}}^{\mathrm{lt}}}\right)}\ . \tag{11}$$

Note that all temperatures are in Kelvin in Eq. 11. $\mathrm{T}_{\mathrm{HP}}^{\mathrm{source}}[\mathrm{t}]$ is equal to $\mathrm{T_{ext}}[\mathrm{t}]$, while $\Psi_{\mathrm{HP}}^{\mathrm{Lorenz}}$ is here set to 0.50. This value is in line with the values greater than 0.50 and equal to 0.61 reported respectively by [49] and [50] for air-source heat pumps supplying district heating networks at equivalent temperature levels. $\Delta \mathrm{T}_{\mathrm{HP}}^{\mathrm{source}}$ corresponds to the temperature glide of the heat source. For the sake of clarity, these parameters are illustrated alongside the heat pump cycle in Fig. 5.

Similarly, the power balance for the heat engine can be written as

$$\begin{aligned}\mathrm{P_{HE}}[\mathrm{t}] &= \dot{\mathrm{Q}}_{\mathrm{HE}}[\mathrm{t}] \cdot \eta_{\mathrm{HE}} && (12)\\ &= \dot{\mathrm{Q}}_{\mathrm{HE}}[\mathrm{t}] \cdot \Psi_{\mathrm{HE}}^{\mathrm{Lorenz}} \cdot \eta_{\mathrm{HE}}^{\mathrm{Lorenz}}[\mathrm{t}] && (13)\\ &= \dot{\mathrm{Q}}_{\mathrm{HE}}[\mathrm{t}] \cdot \Psi_{\mathrm{HE}}^{\mathrm{Lorenz}} \cdot \frac{\overline{\mathrm{T}}_{\mathrm{H}} - \overline{\mathrm{T}}_{\mathrm{C}}[\mathrm{t}]}{\overline{\mathrm{T}}_{\mathrm{H}}}\ , && (14)\end{aligned}$$

$\overline{\mathrm{T}}_{\mathrm{H}}$ and $\overline{\mathrm{T}}_{\mathrm{C}}[\mathrm{t}]$ are the mean source and sink temperatures, defined this time as

$$\overline{\mathrm{T}}_{\mathrm{H}} = \frac{\mathrm{T}_{\mathrm{TES}}^{\mathrm{ht}} - \mathrm{T}_{\mathrm{TES}}^{\mathrm{lt}}}{\ln\left(\frac{\mathrm{T}_{\mathrm{TES}}^{\mathrm{ht}}}{\mathrm{T}_{\mathrm{TES}}^{\mathrm{lt}}}\right)}\ ,\ \ \overline{\mathrm{T}}_{\mathrm{C}} = \frac{(\mathrm{T}_{\mathrm{HE}}^{\mathrm{sink}}[\mathrm{t}] + \Delta \mathrm{T}_{\mathrm{HE}}^{\mathrm{sink}}) - \mathrm{T}_{\mathrm{HE}}^{\mathrm{sink}}[\mathrm{t}]}{\ln\left(\frac{\mathrm{T}_{\mathrm{HE}}^{\mathrm{sink}}[\mathrm{t}] + \Delta \mathrm{T}_{\mathrm{HE}}^{\mathrm{sink}}}{\mathrm{T}_{\mathrm{HE}}^{\mathrm{sink}}[\mathrm{t}]}\right)}\ . \tag{15}$$

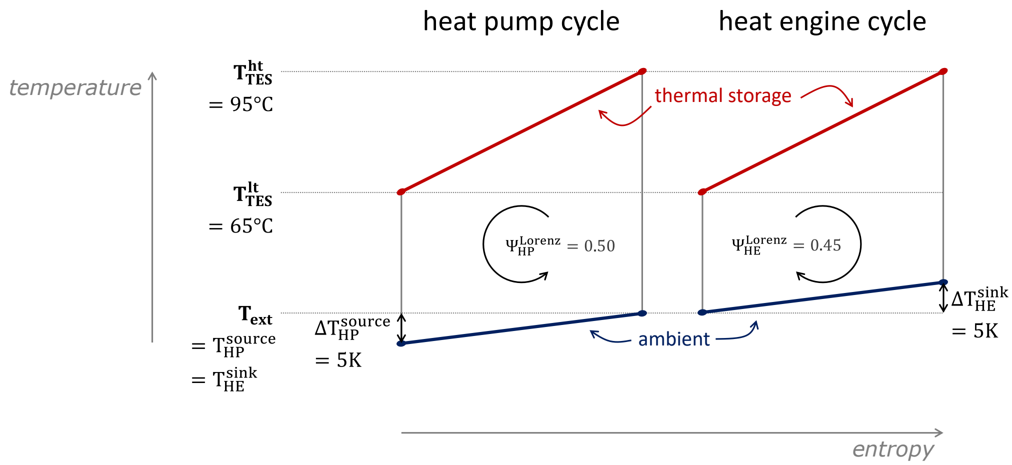

Figure 5: Schematic representation of the heat pump and heat engine models.

Again, all temperatures in Eq. 15 are in Kelvin. $T_{HE}^{sink}[t]$ is equal to $T_{ext}[t]$, while Ψ_{HE}^{Lorenz} is here set to 0.45 [9, 29, 51]. ΔT_{HE}^{sink} corresponds to the temperature glide of the heat sink. For the sake of clarity, these parameters are illustrated alongside the heat engine cycle in Fig. 5.

Please note that linear programming models cannot directly represent the additional energy consumption linked to the dynamic effects of the heat pump and heat engine, such as cold starts, transients or defrost cycles. This model therefore assumes that such effects are quantified indirectly through the coefficients Ψ_{HP}^{Lorenz} and Ψ_{HE}^{Lorenz}, whose values are slightly lower than the nominal values reported in the literature. This approach is similar to assigning a seasonal coefficient of performance to a heat pump, instead of its nominal value.

Finally, the inequality constraints for maximum power flows in the heat pump and heat engine are formulated as

$$P_{HP}[t] \leq P_{HP}^{nom} = \frac{\dot{Q}_{HP}^{nom}}{COP_{HP}^{nom}} \tag{16}$$

$$P_{HE}[t] \leq P_{HE}^{nom} \tag{17}$$

The electrical power of the heat pump is chosen as the upper limit instead of the thermal power because the limiting factor in a real machine is the nominal power of the compressor drive. The value of COP_{HP}^{nom} is established for a source temperature of 15°C.

2.3.3. Thermal energy storage

The thermal energy storage system consists of two water tanks—one for hot water and one for cold. While this design is more costly, it eliminates the constraints related to thermocline degradation found in single stratified tanks (mixing due to fluid circulation, convection and diffusion).

In the model, the thermal storage is the only component whose dynamics is taken into account (via the state-of-charge). The charging $\dot{Q}_{tes}^{ch}$ and discharging $\dot{Q}_{tes}^{disch}$ heat flow rates are related to the self-discharge losses with the following ordinary differential equation:

$$\frac{d}{dt}SOC_{TES}(t) = -k_{self-discharge} \cdot SOC_{TES}(t) + 100 \cdot \frac{\left(\dot{Q}_{tes}^{ch}(t) - \dot{Q}_{tes}^{disch}(t)\right)}{E_{TES}^{nom}} \quad , \qquad (18)$$

where the coefficient $k_{self-discharge}$ represents the self-discharge losses. Formulated in discrete time with an hourly resolution, this equation is written as:

$$SOC_{TES}[t] = \sqrt[24]{1 - L_{TES}} \cdot SOC_{TES}[t-1] + 100 \cdot \frac{\left(\dot{Q}_{tes}^{ch}[t] - \dot{Q}_{tes}^{disch}[t]\right)}{E_{TES}^{nom}} \quad , \qquad (19)$$

where L_{TES} stands for the self-discharge losses and is expressed in %/24 h (which explains the twenty-fourth root). The annual cyclic constraint is imposed as follows:

$$SOC_{TES}[1] = \sqrt[24]{1 - L_{TES}} \cdot SOC_{TES}[8760] + 100 \cdot \frac{\left(\dot{Q}_{tes}^{ch}[1] - \dot{Q}_{tes}^{disch}[1]\right)}{E_{TES}^{nom}} \qquad (20)$$

Due to the lack of information, a value of 5 %/24 h is chosen for L_{TES} (conservative value which could prevent from long term storage). The sensitivity analysis in Section 3.4 will show that this parameter has in any case very little influence on overall performance.

Note that the hypothesis of constant storage temperature raises questions when modelling the storage losses. In reality, any thermal loss in sensible heat storage causes a temperature drop (to which these losses are actually proportional). In this model, the self-discharge losses are instead proportional to the amount of energy stored and they only affect that quantity (not the temperature). For example, in the absence of charge/discharge cycles, if the storage is 100 % charged on day one, it is only 95 % charged the next day, 60 % charged after ten days and 20 % charged after a month. However, the storage temperature would remain unchanged. Modelling the impact of temperature fluctuation would introduce non-linearities into the model, and this degree of precision is probably not necessary in view of the scope of the study. Yet, in order to assess the impact of this hypothesis, future work on this case study would necessitate a more accurate model considering the dynamics of the storage temperature.

As constraints preventing simultaneous charging and discharging cause non-linearities, these are not used here. However, such phenomenon does not affect the state of charge since only the net heat flow rate counts in Eq. 19. Moreover, it can be eliminated when post-processing the results (only the net value is retained). Finally, there are no constraints on the maximum charge and discharge heat flow rates (these are actually constrained by the operations of the heat pump and heat engine). Still, the following constraint does apply to the state of charge:

$$0\% \leq \mathrm{SOC_{TES}}[\mathrm{t}] \leq 100\% \tag{21}$$

2.3.4. Photovoltaic system

The only flow variable for optimisation concerning the photovoltaic system is the power curtailment $\mathrm{P_{PV}^{crt}}$. This is defined as the deliberate reduction of photovoltaic power generation when the system is capable of producing more electricity. This is constrained by the following inequality:

$$0 \leq \mathrm{P_{PV}^{crt}}[\mathrm{t}] \leq \mathrm{P_{PV}}[\mathrm{t}] \tag{22}$$

In Eq. 22, $\mathrm{P_{PV}}[\mathrm{t}]$ is obtained as

$$\mathrm{P_{PV}}[\mathrm{t}] = \mathrm{P_{PV}^{dless}}[\mathrm{t}] \cdot \mathrm{P_{PV}^{nom}} \ , \tag{23}$$

with $\mathrm{P_{PV}^{dless}}[\mathrm{t}]$ the dimensionless photovoltaic power generated by nPro [35] for 30° tilt angle and 0° azimuth (see Fig. 3). The model assumes mono-crystalline modules with an efficiency of 21 % at 25°C and a temperature coefficient of 0.36 %/°C. The inverter efficiency is 96 %.

2.3.5. *Energy balances at the electrical and thermal nodes*

The energy balance at the electrical node is written as:

$$\mathrm{P}_{\mathrm{grid}}^{\mathrm{abs}}[\mathrm{t}] + \mathrm{P}_{\mathrm{PV}}[\mathrm{t}] + \mathrm{P}_{\mathrm{HE}}[\mathrm{t}] = \mathrm{P}_{\mathrm{load}}[\mathrm{t}] + \mathrm{P}_{\mathrm{HP}}[\mathrm{t}] + \mathrm{P}_{\mathrm{grid}}^{\mathrm{inj}}[\mathrm{t}] + \mathrm{P}_{\mathrm{PV}}^{\mathrm{crt}}[\mathrm{t}] \quad (24)$$

In contrast to the thermal energy storage, bi-directional flows with the grid (simultaneous absorption and injection) must be prevented. In fact, due to the difference between retail and feed-in tariffs, if the retail price is below feed-in tariff, it would be virtually possible to generate profit by directly re-injecting the absorbed electricity back into the grid. Such phenomenon would of course not happen with the economic model described in Section 2.2 but could occur with dynamic retail tariffs, as it will be tested in Section 3.3.2 (e.g. negative retail tariff combined with zero feed-in tariff). In order to prevent that, a quadratic constraint is added:

$$\mathrm{P}_{\mathrm{grid}}^{\mathrm{abs}}[\mathrm{t}] \cdot \mathrm{P}_{\mathrm{grid}}^{\mathrm{inj}}[\mathrm{t}] = 0 \quad (25)$$

Although it slows down the linear model, Eq. 25 is necessary for the consistency of the results.

For its part, the energy balance at the thermal node is as follows:

$$\dot{\mathrm{Q}}_{\mathrm{HP}}[\mathrm{t}] + \dot{\mathrm{Q}}_{\mathrm{TES}}^{\mathrm{disch}}[\mathrm{t}] = \dot{\mathrm{Q}}_{\mathrm{load}}[\mathrm{t}] + \dot{\mathrm{Q}}_{\mathrm{HE}}[\mathrm{t}] + \dot{\mathrm{Q}}_{\mathrm{TES}}^{\mathrm{ch}}[\mathrm{t}] \quad (26)$$

2.4. *Uncertainty quantification*

Section 3.4 will look at the sensitivity of the annualised energy cost to technical and operational uncertainties for one of the optimum designs obtained. The optimisation model presented in Section 2.3 was therefore first modified to allow a given design to be tested and only an optimal scheduling of the energy system to be carried out.

The uncertainties are then propagated into the energy system using the `RHEIA` package [52], which based on polynomial chaos expansion. This technique aims to construct a surrogate model (based on orthonormal polynomials) that can be used to directly deduce the statistical moments of interest, such as the mean, variance, and Sobol indices. Compared with Monte Carlo simulations, polynomial chaos requires much less model evaluations. This number is proportional to the number of uncertainties considered and the degree of the polynomial model. In this work, a third-order polynomial was employed to guarantee sufficient accuracy.

As described in Section 3.4, eight uncertainties relating to climatic conditions, demand data, and to the performance of the different components have been considered. These are reported in Table 4. The aim is to identify which parameters drive uncertainty in the energy cost and to understand how the design of the energy system could be improved. To identify these parameters, their total-order Sobol indices will be quantified with the `RHEIA` package [52]. Each index represents the contribution of the uncertain parameter to the global variance on the annualised energy cost.

Table 4: Technical and operational uncertainties considered in the sensitivity analysis.

Parameter	**Symbol**	**Uncert.**	**Unit**	**Reference**
Nominal electric load (plug loads and cooling)	$\mathrm{P}_{\mathrm{load}}^{\mathrm{nom}}$	±15	$\%_{\mathrm{rel}}$	[6]
Nominal thermal load (space heating)	$\dot{\mathrm{Q}}_{\mathrm{load,sh}}^{\mathrm{nom}}$	±15	$\%_{\mathrm{rel}}$	[6]
Nominal thermal load (domestic hot water)	$\dot{\mathrm{Q}}_{\mathrm{load,dhw}}^{\mathrm{nom}}$	±15	$\%_{\mathrm{rel}}$	[6]
HP fraction of Lorenz efficiency	$\Psi_{\mathrm{HP}}^{\mathrm{Lorenz}}$	±15	$\%_{\mathrm{rel}}$	[45]
HE fraction of Lorenz efficiency	$\Psi_{\mathrm{HE}}^{\mathrm{Lorenz}}$	±15	$\%_{\mathrm{rel}}$	[51]
External temperature	$\mathrm{T}_{\mathrm{ext}}$	±0.5	K	[6]
Photovoltaic production (irradiance)	P_{PV}	±7.8	$\%_{\mathrm{rel}}$	[6]
TES self-discharge	$\mathrm{L}_{\mathrm{TES}}$	±50	$\%_{\mathrm{rel}}$	sensitivity

3. Results

This section first introduces the optimum system designs over the range of considered $\mathrm{CAPEX}_{\mathrm{HP}}$, $\mathrm{CAPEX}_{\mathrm{HE}}$ and $\mathrm{CAPEX}_{\mathrm{TES}}$. Then, to illustrate the seasonal trends, the system operations are analysed over the typical year for one specific design. After that, parametric analyses are conducted to assess the impact of non-zero feed-in tariff and dynamic retail tariff on the system design and cost. The sensitivity analysis is then carried out to assess which parameters drive the uncertainty on the annualised energy cost. Eventually, the results from Brussels are compared with the reference results from Pisa to characterise the impact of climatic conditions on the design and operations of the system.

3.1. Optimum system design based on investment costs

Fig. 6 depicts the capacities of the heat pump, storage, heat engine and photovoltaic system that minimise the annual energy cost, over the range of considered investment costs. Since the design trends are monotonic between $\text{CAPEX}_{\text{TES}} = 20$ €/kWh$_{\text{th}}$ and 40 €/kWh$_{\text{th}}$, results for $\text{CAPEX}_{\text{TES}} = 30$ €/kWh$_{\text{th}}$ are not reported for the sake of clarity.

First observation is that the more expensive the heat pump, the smaller its capacity (Fig. 6a). This downsizing, aimed at maximising its capacity factor (ratio between actual annual energy production and maximum possible production) and at reducing the associated investment cost, is made possible by an increase in storage capacity (Fig. 6b). The model anticipates peak thermal loads in the morning and evening (Fig. 3) by distributing heat production over the day, so that it can then rapidly discharge the storage at peak times (further illustrated in Section 3.2 and Fig. B.2). Conversely, the more expensive the storage, the larger the heat pump (Fig. 6a). Overall, this clearly illustrates that, as well as shifting photovoltaic production, the thermal energy storage acts as a buffer to downsize the heat pump and increase its capacity factor. Another advantage that comes with the storage, which is not taken into account in the economic model considered in this work, is that it limits the number of times the heat pump is started up, which increases the service life of its compressor.

On the other hand, the storage capacity is affected to a lesser extent by CAPEX_{HE} (the more expensive, the lower the capacity). This highlights that the storage capacity is driven first and foremost by heat production and demand, rather than electricity demand. In other words, thermal storage is primarily sized to meet heat requirements.

Another key result is that for most of the costs considered, a heat engine is installed to

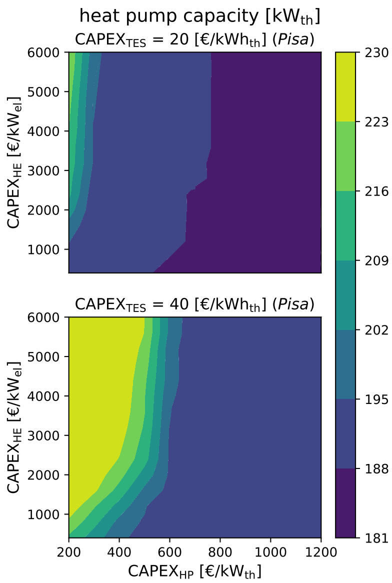

(a) Installed heat pump capacity.

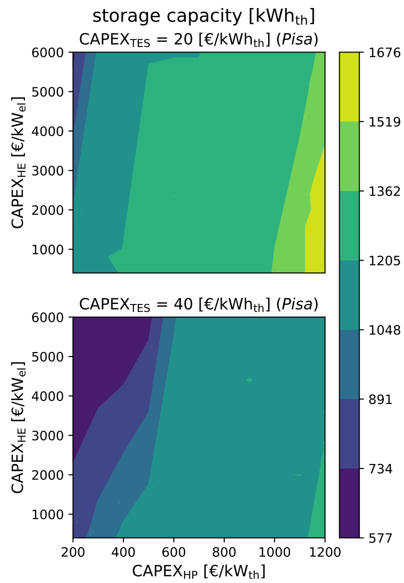

(b) Installed thermal storage capacity

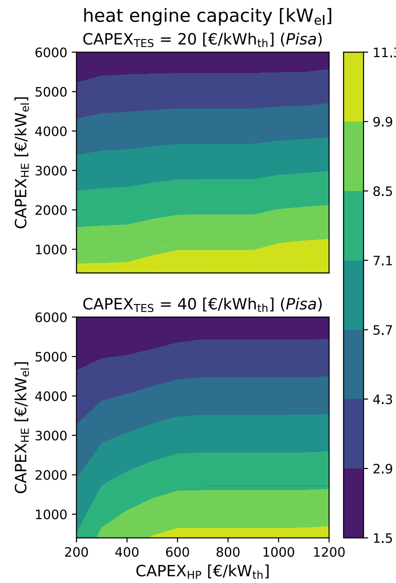

(c) Installed heat engine capacity.

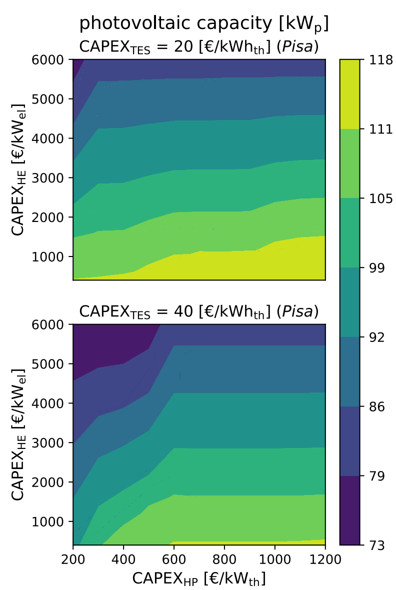

(d) Installed photovoltaic capacity.

Figure 6: Optimum system design based on the investment costs considered. The colourmaps depict the installed capacities. The x-axis represents the costs considered for the heat pump, the y-axis the costs of the heat engine and the top and bottom maps illustrate two different storage costs.

provide electricity storage (Fig. 6c). Its capacity is mainly driven by $\mathrm{CAPEX_{HE}}$, but gets affected by $\mathrm{CAPEX_{HP}}$ as $\mathrm{CAPEX_{TES}}$ increases.

To illustrate the role of the heat engine, Figs. 7a and 7b depict respectively the fraction of total electricity demand which is covered by the heat engine and the fraction of photovoltaic production which is curtailed. The correlation between the latter and the heat engine capacity is evident: as the capacity increases, the curtailed fraction drops from about 17 % down to less than 6 %. This clearly demonstrates the benefits of the heat engine in limiting the waste of renewable energy potential. Nonetheless, this observation must be put into perspective with the electricity demand, which is only between 5.6 % and 21.3 % covered by the heat engine. As it will also be illustrated, these relatively low values are due to the fact that the heat engine is only used for part of the year, when photovoltaic production is high and thermal demand is low.

It should also be noted that the lower the storage capacity, the more the increase in $\mathrm{CAPEX_{HE}}$ tends to increase the heat pump capacity. This is because as the capacity of the heat engine decreases, the amount of storage required decreases (i.e. reduced electricity storage), which, as mentioned above, requires an increase in the capacity of the heat pump. However, this impact on the capacity of the heat pump is much less pronounced than that of $\mathrm{CAPEX_{HP}}$.

Let us thus conclude that although it has a role to play, the heat engine produces a limited amount of electricity, covering in any case less than 21 % of the total electricity demand.

As far as the photovoltaic system is concerned, the installed capacity is between 73 and 118 $\mathrm{kW_p}$ in all cases, i.e. less than 5.9 $\mathrm{kW_p}$/dwelling, which is totally plausible. In Fig. 6d, the synergy between the photovoltaic capacity and $\mathrm{CAPEX_{HE}}$ is also well visible: the more expensive, the smaller the photovoltaic system. Fig. 6d perfectly illustrates the fact that a minimum photovoltaic capacity is required to meet heating needs (about 80 $\mathrm{kW_p}$), and that any additional capacity will be used to meet electricity needs, since it will be directly proportional to the heat engine capacity. To sum up, the minimum capacity of the

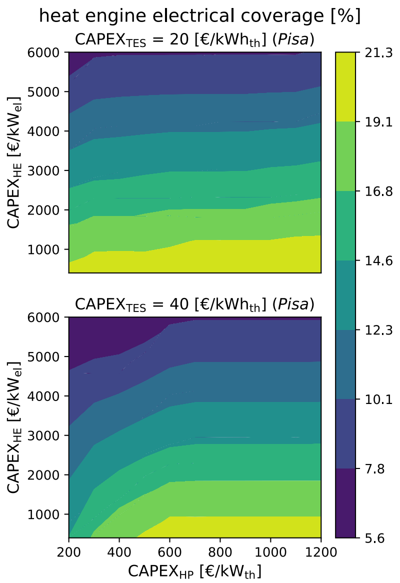

(a) Fraction of electricity consumption covered by the heat engine.

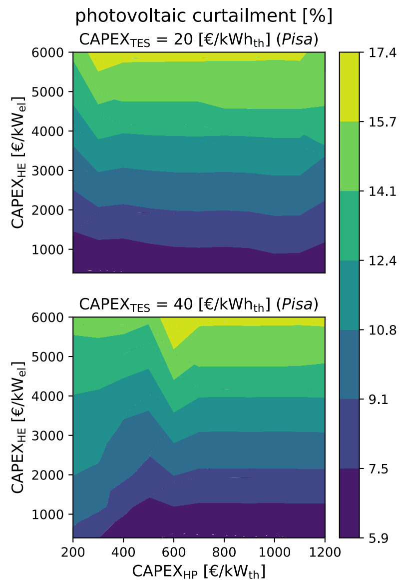

(b) Fraction of curtailed photovoltaic production.

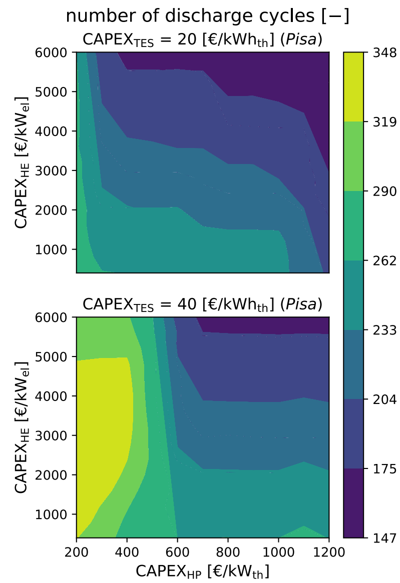

(c) Number of discharge cycles for the storage.

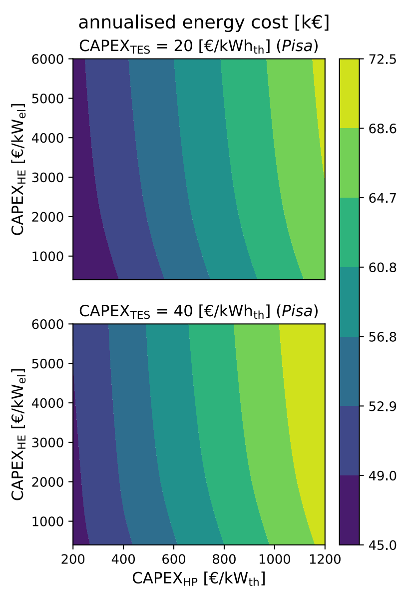

(d) Annualised energy cost.

Figure 7: Performance indicators for the system operations based on the investment costs considered. The x-axis represents the costs considered for the heat pump, the y-axis the costs of the heat engine and the top and bottom maps illustrate two different storage costs.

photovoltaic system is dictated by heat demand, and any additional capacity is accompanied by an increase in heat engine capacity to meet electricity demand.

One can also observe that when the storage cost is low, the higher CAPEX_{HP}, the larger the photovoltaic capacity. This can be explained by the fact that, as the cost of the heat pump will weigh more heavily in the annualised energy cost, it is preferable to gain in self-production in order to reduce grid electricity consumption and reduce the associated costs (the electricity term E in Eq. 3). In addition, the capacity of the heat pump can be reduced by self-consuming more photovoltaic electricity thanks to the thermal storage.

Fig. 7c depicts the number discharge cycles. This number is between 147 and 348, and seems to be a function of CAPEX_{HE}. As illustrated by the operational analysis in Section 3.2, full charge/discharge cycles are performed daily during the electricity storage period (spring/summer), due to the coupling with the photovoltaic system. On the other hand, during the cold season (autumn/winter), storage essentially acts as a buffer between the heat pump and thermal demand (few electrical discharges).

Therefore, as CAPEX_{HE} decreases, the capacities of the heat engine and of the photovoltaic system increase (see Figs. 6c and 6d), which extends the period of electrical discharges, and therefore increases the number of cycles associated with this. For its part, the number of cycles linked to the buffer role for heat management remains more or less unchanged. Fig. 7c also shows that, as the cost of storage increases, its capacity decreases, which increases the number of discharge cycles.

Fig. 7d finally depicts the annualised energy cost. It clearly demonstrates that the system cost is driven by CAPEX_{HP} and is much less sensitive to $\text{CAPEX}_{\text{TES}}$ and CAPEX_{HE}.

As a conclusion to this section, installing a heat engine (and thus a proper Carnot battery) can be financially profitable in residential applications where the thermal demand is covered by a heat pump coupled to thermal storage and a photovoltaic system. Nevertheless, the main driver for installing the photovoltaic system and thermal storage is the thermal demand, as confirmed by the extreme case where no heat engine is installed due to the large $CAPEX_{HE}$. Therefore, if a photovoltaic system and thermal storage are to be installed, adding a heat engine to cover part of the electricity consumption can be a profitable option.

3.2. Analysis of daily and seasonal operations

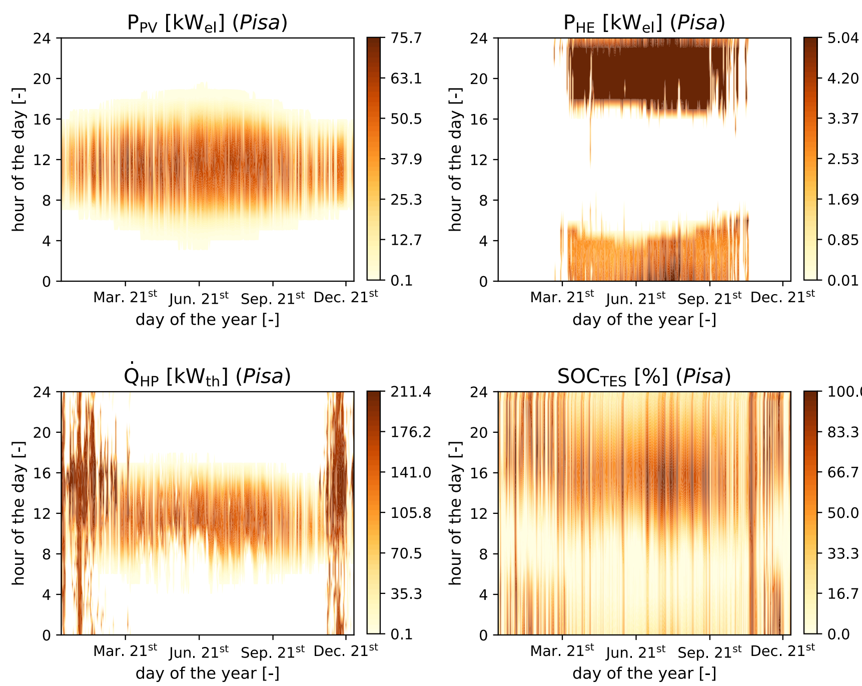

Figure 8: Temporal heatmaps representing the system operations for Pisa (photovoltaic power production P_{PV}, heat engine power production P_{HE}, heat pump thermal production $\dot{Q}_{HP}$ and storage state-of-charge SOC_{TES}). The the days of the year are plotted along the x-axis, and hours of the day are plotted along the y-axis.

To understand how the different components are operated according to the system boundary conditions, the system operations are analysed over the full year. To do so, a representative design must be selected. The design corresponding to the case $CAPEX_{HP}$ = 600 €/kW_{th}, $CAPEX_{HE}$ = 2400 €/kW_{el} and $CAPEX_{TES}$ = 30 €/kWh_{th} was selected because these values reflect the current costs considered in the literature [9, 29, 31]. Although the magnitude of the power flows in the other designs is different (due to different nominal capacities), the trends are the same. Fig. 8 shows the daily and seasonal operations of the system components across the entire year. In addition, Table 5 provides various performance indicators for each season. Eventually, the system design is reported in Table 6. As complements to Fig. 8, Figs. B.1 and B.2 in Appendix B depict the full system operations over the 24 h of two representative days in summer and winter.

Table 5: Seasonal operations and performance indicators for Pisa. The considered design is for $CAPEX_{HP}$ = 600 €/kW_{th}, $CAPEX_{HE}$ = 2400 €/kW_{el} and $CAPEX_{TES}$ = 30 €/kWh_{th}. Astronomical seasons are here considered. During winter, the slight difference between heat production and demand is due to the thermal losses in the storage. N_{cycles} is the number of charging/discharging cycles of the thermal storage and E^{abs}_{grid} is the grid electricity consumption.

Parameter	**Unit**	**Winter**	**Spring**	**Summer**	**Autumn**	**Annual**
E^{th}_{load}	MWh_{th}	146.2	26.5	14.7	82.6	270.0
E_{HP}	MWh_{th}	148.6	75.5	86.5	104.2	414.8
COP_{HP}	-	2.56	3.00	3.50	2.66	2.82
E^{el}_{load}	MWh_{el}	17.2	15.4	22.8	17.0	72.4
E_{HE}	MWh_{el}	0.05	3.72	4.81	1.57	10.15
η_{HE}	%	8.82	7.83	6.95	7.86	7.40
$COP_{HP} \cdot \eta_{HE}$	%	22.6	23.5	24.3	20.9	20.9
N_{cycles}	-	56.4	52.4	63.8	44.7	217.3
E_{PV}	MWh_{el}	22.1	39.5	41.7	23.1	126.4
E^{abs}_{grid}	MWh_{el}	53.0	3.4	3.9	31.6	91.9

Fig. 8 first clearly confirms that the heat engine is mostly used during spring and summer seasons to complement the photovoltaic production (electrical discharge when no production). Almost no electrical discharge occurs during winter while summer is the season with the largest heat engine production (see Table 5). Another observation is that the heat engine runs at part load during the morning, mainly because of the lower loads at that moment (see Figs. 3 and B.1).

Table 6: Nominal system design for Pisa. The considered design is for $CAPEX_{HP}$ = 600 €/kW_{th}, $CAPEX_{HE}$ = 2400 €/kW_{el} and $CAPEX_{TES}$ = 30 €/kWh_{th}.

Parameter	**Symbol**	**Value**	**Unit**
Heat pump capacity	$\dot{Q}^{nom}_{HP}$	189.5	kW_{th}
Storage capacity	E^{nom}_{TES}	1203	kWh_{th}
Total storage volume	V^{nom}_{TES}	70.8	m^3
Heat engine capacity	P^{nom}_{HE}	5.04	kW_{el}
Photovoltaic capacity	P^{nom}_{PV}	94.4	kW_p
Annualised energy cost	AEC	56.9	k€

The correlation between the heat pump operations and photovoltaic production is also well visible in Figs. 8 and B.1. In spring and summer, the heat pump is mostly driven by the photovoltaic system. Since the thermal demand is low at that moment, the produced heat is directly charged into the storage, to be later discharged as electricity with the heat engine. It is also interesting to note that when the heat pump matches the photovoltaic production, it operates mostly at part load (see Figs. 8 and B.1). It would therefore be relevant in future work to assess the impact of part-load efficiency degradation on the results obtained with this linear model.

Instead, during cold autumn and winter days, the heat production is spread all over the day so that the heat pump runs at constant load (Figs. 8 and B.2). Due to the limited photovoltaic potential at that period, most of the electricity needed to run the heat pump is absorbed from the grid.

In Fig. 8, the sate-of-charge also gives an overview of the storage operations. It is clear that it is used to shift photovoltaic production during the summer, whereas in winter it acts more as a buffer between heat production and heat demand (it is still used as a complement to photovoltaics, but to a lesser extent). This can be further observed in Figs. B.1 and B.2.

We also note that storage is primarily used for daily buffering, not for longer-term storage. This means that the perfect annual foresight assumption introduced into the model does not bias the results (an accurate forecast of energy demand and photovoltaic production on a daily basis is realistic). If, on the other hand, it were used for longer-term storage (weekly or seasonal), this assumption would be more questionable.

The key message from this seasonal operational analysis is that the heat engine is only used when photovoltaic energy is abundant and demand for heat is low (essentially summer and spring). On the other hand, when photovoltaic production is lower and demand for heat is higher (autumn and winter), priority is given to heat storage, as this is more efficient (and therefore more economically profitable) than electricity storage. One way of increasing the overall efficiency of the energy system would therefore be to reduce the temperature of the heat produced in winter in order to increase the COP of the heat pump (the motivation for a value of 95°C was discussed in Section 2.1).

However, as sensible heat storage is considered, a reduction in the high temperature would lower the storage density (Eq. 1), and thus the storage capacity for a fixed volume (Eq. 2). To maintain capacity, the storage volume would be increased, raising the investments costs, whereas the increase in COP due to the decrease in temperature was precisely intended to reduce the annualised energy cost. A dedicated techno-economic study is therefore needed to find the optimum temperature.

3.3. Impact of electricity pricing model

In order to assess the impact of the electricity pricing system, two parametric analyses are carried out. The first looks at the impact of a non-zero feed-in tariff, in contrast to the results above. The second looks at a dynamic (rather than constant) retail tariff, and more specifically at the level of fluctuation required to observe financial gains from the energy arbitrage mechanism.

3.3.1. Non-zero feed-in tariff

For the case of a 0.05 €/kWh_{el} feed-in tariff, Figs. 9a and 9b illustrate the relative deviation in nominal capacity for the photovoltaic system and heat engine, with respect to the reference designs with zero feed-in tariff introduced in Section 3.1. The deviation in heat pump capacity is not depicted because it stays within a narrow range (-7.4 % to +6.8 %). Storage is not shown either because the trends are rather irregular (non-uniform increases and decreases on the colourmap) and are not key to discuss the effect of non-zero feed-in tariff.

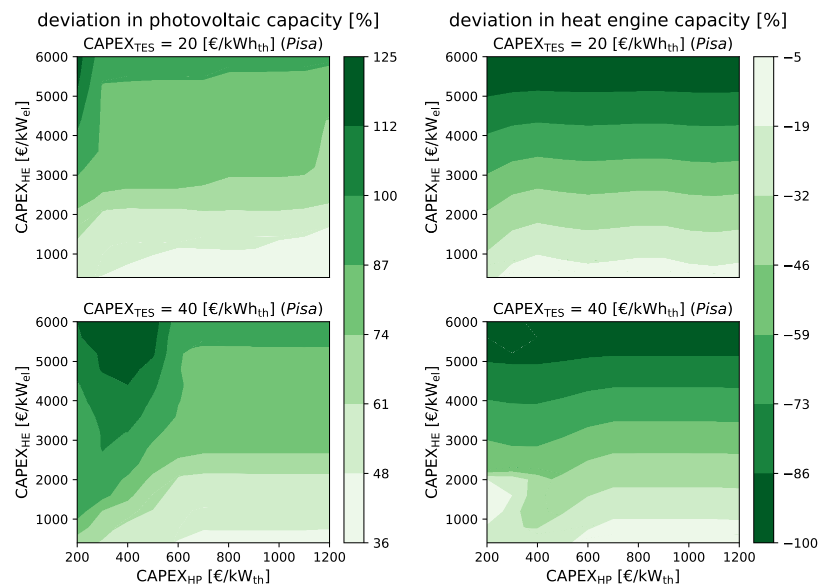

(a) Photovoltaic capacity.

(b) Heat engine capacity.

Figure 9: Deviations in installed capacities due to non-zero feed-in tariff. The colourmaps depict the relative deviations. The x-axis represents the costs considered for the heat pump, the y-axis the costs of the heat engine and the top and bottom maps illustrate two different storage costs.

Results show that the photovoltaic capacity is largely increased. This shows that a non-zero feed-in tariff, although significantly lower than the retail tariff (0.05 €/kWh against 0.30 €/kWh), is clearly beneficial to the installation of photovoltaic systems. On the other hand, the capacity of the heat engine is relatively reduced compared with the reference case. It is even removed for higher $CAPEX_{HE}$.

As the increase in photovoltaic capacity is counterbalanced by the reduction in heat engine capacity, it is not possible to conclude directly whether the non-zero feed-in tariff reduces dependence on the grid. Fig. 10a therefore depicts the relative deviation in electricity consumption from the grid. Clearly, despite the reduction in heat engine capacity, electricity consumption is decreasing, meaning that energy self-sufficiency is increasing.

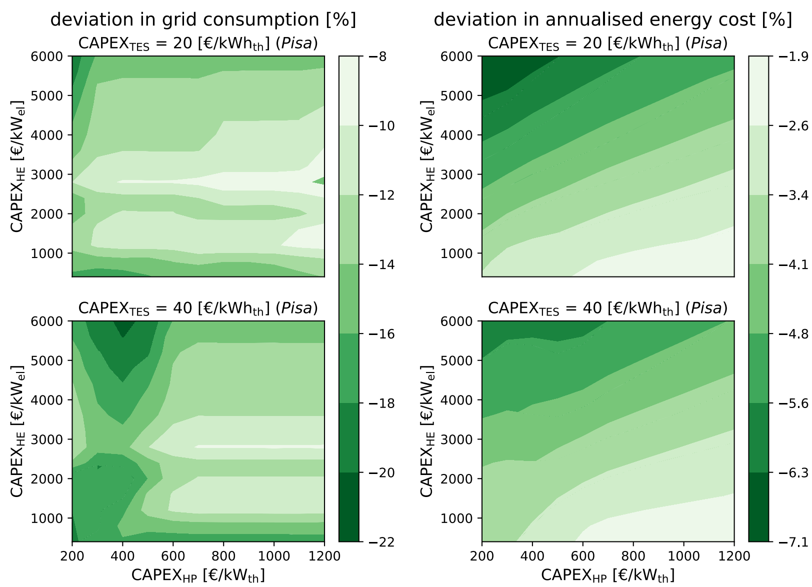

(a) Grid electricity consumption.

(b) Annualised energy cost.

Figure 10: Deviations in performance indicators due to non-zero feed-in tariff. The colourmaps depict the relative deviations. The x-axis represents the costs considered for the heat pump, the y-axis the costs of the heat engine and the top and bottom maps illustrate two different storage costs.

Fig. 10b finally depicts the relative deviation in annualised energy cost. The gain is relatively limited, as it reaches maximum -7.1 %. This illustrates that from a financial perspective, non-zero feed-in tariff is not a game changer, meanwhile it significantly affects the electrical storage capacity. Scharrer et al. [30], who considered a retail price of 0.36 €/kWh and a feed-in tariff of 0.06 €/kWh, drew similar conclusion.

3.3.2. Dynamic retail tariff

Benefiting from dynamic (or "variable") energy prices is an argument frequently put forward to increase the profitability of domestic energy storage projects [53, 54]. Conceptually, storage allows for purchasing energy from the grid when costs are low (due to low market demand and/or high renewable production) and then discharging it to meet demand when prices are high. This is similar to the energy arbitrage mechanism.

To assess whether such pricing model would be profitable to residential Carnot batteries, a parametric analysis was carried out to study how the level of fluctuation affects the optimum design. For this work, this level has been defined as

$$\mathrm{CV}(\mathrm{p_{elec}}) = \frac{\sigma(\mathrm{p_{elec}})}{\mu(\mathrm{p_{elec}})} \ , \tag{27}$$

which is the coefficient of variation (ratio between standard deviation σ and mean μ) of the electricity price $\mathrm{p_{elec}}$ over the typical year.

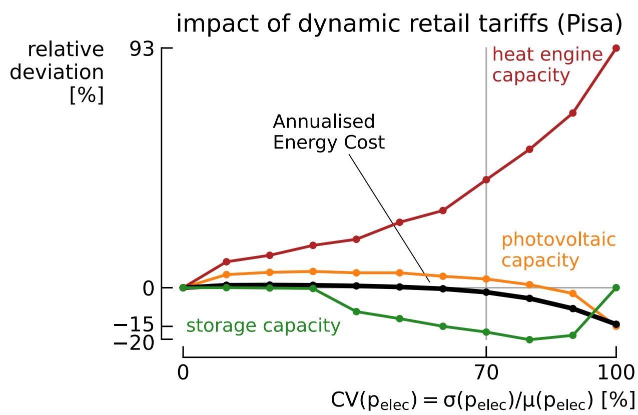

Figure 11: Relative deviation in annualised energy cost, photovoltaic, storage and heat engine capacities for different coefficients of variation of retail tariffs. The design corresponding to case $\mathrm{CAPEX_{HP}} = 600$ €/kW$_{\mathrm{th}}$, $\mathrm{CAPEX_{HE}} = 2400$ €/kW$_{\mathrm{el}}$ and $\mathrm{CAPEX_{TES}} = 30$ €/kWh$_{\mathrm{th}}$ was selected for the analysis.

For this analysis, the case $\mathrm{CAPEX_{HP}} = 600$ €/kW$_{\mathrm{th}}$, $\mathrm{CAPEX_{HE}} = 2400$ €/kW$_{\mathrm{el}}$ and $\mathrm{CAPEX_{TES}} = 30$ €/kWh$_{\mathrm{th}}$ was also selected. Fig. 11 depicts the relative deviation in annualised energy cost, photovoltaic, thermal energy storage and heat engine capacities for coefficients of variation from 0 % to 100 %. First observation is that below 70 %, there is no financial gain. This is mainly due to high retail tariffs in autumn and winter, when demand for electricity from the grid is highest (important heat consumption and low photovoltaic production). As illustrated in Fig. 4, a daily effect is also at work: prices are higher when demand for energy is higher (morning and evening peaks).

To compensate for the increase in the share of the cost of electricity in the annualised energy cost, the size of the engine is increased in order to provide greater electrical self-sufficiency. Note also that the storage capacity tends to decrease. For their part, the capacity of the photovoltaic system and the annualised energy cost remain relatively constant.

Instead, when the coefficient of variation of the electricity price is greater or equal to 70 %, financial gain starts to occur (around -15 % in annualised energy cost for a level of 100 %). While photovoltaic capacity is falling (-15 %), the heat engine capacity is rising sharply: it produces considerably more electricity. This suggests that low-cost (and even negative price) electricity is charged into the storage, and then discharged to meet energy demand when retail tariffs are high (morning and evening peaks). In fact, as the level of fluctuation in electricity price increases, the origin of the profitability of the Carnot battery shifts progressively from photovoltaic load shifting to energy arbitrage. This result therefore shows that if the electricity price fluctuates greatly, arbitrage via the Carnot battery is the most financially attractive option, despite its limited efficiency.

However, the above results must be seen in the context of historical fluctuation levels. Indeed, the level of fluctuation on the day-ahead market as defined in Eq. 27 has not exceeded 70 % in most European countries, with the exception of the years of the energy crisis. It is also important to point out that these levels of fluctuation are accompanied by a fall in installed photovoltaic capacity, and therefore in the production of decentralised renewable energy. In the context of the energy transition, this seems counterproductive. What is more, reducing the distributed generation of photovoltaic electricity should have a retroactive effect on fluctuations in electricity prices.

Finally, such high levels of fluctuation in retail tariffs for residential customers raise questions. Households without energy storage systems could be severely penalised. The plausibility of this type of scenario is therefore questionable.

3.4. Sensitivity to uncertainties

The effect of technical and operational uncertainties on the financial performance of residential Carnot batteries was assessed through a global sensitivity analysis. The design corresponding to case $CAPEX_{HP}$ = 600 €/kW_{th}, $CAPEX_{HE}$ = 2400 €/kW_{el} and $CAPEX_{TES}$ = 30 €/kWh_{th} was selected for the analysis (see Table 6 for capacities). The uncertainties affecting the different parameters are reported in Table 4. These were propagated through the model using Polynomial Chaos Expansion, as explained in Section 2.4. Since the design is fixed in this analysis, only the electricity-related expenditures (i.e. electricity consumption) affect the annualised energy cost.

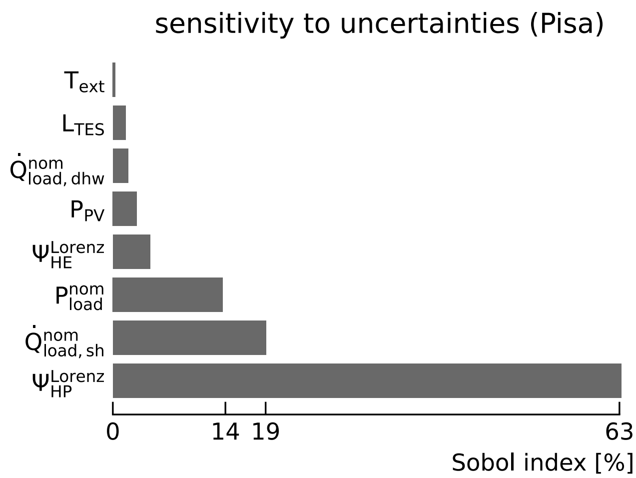

Figure 12: Sobol indices corresponding to the uncertain parameters considered in the sensitivity analysis (Table 4). The design corresponding to case $CAPEX_{HP}$ = 600 €/kW_{th}, $CAPEX_{HE}$ = 2400 €/kW_{el} and $CAPEX_{TES}$ = 30 €/kWh_{th} was selected for the analysis.

Fig. 12 depicts the Sobol indices for each uncertain parameter. Each index represents the contribution of the uncertain parameter to the global variance on the annualised energy cost. Clearly, this cost is most sensitive to space heating related parameters, and to a lesser extent to the electrical load. With a Sobol index of 63 %, the heat pump fraction of Lorenz efficiency Ψ^{Lorenz}_{HP} is the primary source of system sensitivity. Next comes the heat load for space heating $\dot{Q}_{load,sh}$. This result is entirely logical given the volume of energy involved. This illustrates the importance of maximising the COP of the heat pump in order to reduce operating costs. In third place comes the electrical load P_{load}, with an index of around 14 %.

The other five parameters have indices below 5 %. These can therefore be considered negligible. The fact that the Sobol index of Ψ_{HE}^{Lorenz} is negligible illustrates that in the event of a major overproduction of photovoltaic electricity, it is still profitable to store this despite the low efficiency (provided the cost of the storage system allows). Indeed, in spring and summer, the average power-to-power efficiency of the Carnot battery, which is equivalent to the product of COP_{HP} and η_{HE}, does not exceed 25 % (see Table 5). If it were not stored, this energy would simply be lost. This observation therefore suggests a reduction in the storage temperature, which would reduce the efficiency of the Carnot battery but increase the COP of the heat pump, thereby reducing operating costs.

It is also interesting to note that the cost of the system is relatively insensitive to the self-discharge losses L_{TES}, despite the wide range of variation considered ($\pm$ 50 $\%_{rel}$). Intuitively, one might think that during the system sizing phase (Section 3.1), these losses (5 %/24 h) prevented long-term storage, which therefore made the system rather insensitive to them (storage is only used on a daily basis). However, this hypothesis can quickly be discarded: a parametric analysis showed that by neglecting self-discharge losses (L_{TES} = 0 %/24h), the designs obtained were relatively unchanged compared with the case L_{TES} = 5 %/24h. The relative deviation in capacity ranged from 0 % for thermal storage to 2.5 % for the heat engine. It can therefore be said that the limited storage capacity, which makes the system rather insensitive to self-discharge losses, is due to its high cost and not to the losses themselves.

From the sensitivity analysis, it can be concluded that in a residential energy system equipped with a photovoltaic system, a heat pump and thermal energy storage, adding a heat engine does not present any real financial risk and can reduce energy bills. Regardless of its efficiency, it will be used in any case to limit curtailment during spring and summer.

3.5. Extending results to other locations

The aim of this section is to extend and generalise the results obtained from the reference case of Pisa to other climatic conditions. To do this, the same study was carried out for the case of Brussels, which has a colder climate (higher heating demand, lower cooling demand) and lower annual solar irradiance. It is also more prone to seasonality (greater difference between winter and summer solstices). The corresponding boundary conditions are depicted in Fig. A.1 in Appendix A. To simplify the analysis, only the significant differences between Pisa and Brussels are discussed. All the corresponding results are given in Appendix A.

In terms of system design, storage capacity is on average lower in Brussels than in Pisa (up to 65 % less). The number of charge/discharge cycles is consequently up to 75 % higher. This reduced need for storage is explained in particular by the lower photovoltaic production and the greater capacity of the heat pump (up to 10 %).

In addition to storage, the capacity of the heat engine is 20 to 100 % lower. As a result, its production covers only 0 to 13 % of the electricity demand, i.e. on average 40 to 100 % less than in Pisa (for high $\mathrm{CAPEX}_{\mathrm{HE}}$, no heat engine is installed). Curtailment is also logically higher in Brussels, since electricity storage capacity is more limited there. This difference in electricity storage capacity is explained in particular by the fact that the period of heat demand for space heating is longer there, while the photovoltaic potential is more concentrated around the summer solstice. Consequently, this reduces the potential period for electricity discharge.

Given the lower photovoltaic potential, which is more concentrated around the warm season, and the higher demand for heat in winter, the annualised energy cost is logically higher in Brussels than in Pisa. This is further amplified by the fact that the COP of the heat pump is lower in Brussels, due to the lower average temperature.

The parametric analysis on electricity tariffs also reveals differences between Brussels and Pisa. In the case of a non-zero feed-in tariff, the capacity of the heat engine decreases much more (it is even removed in many cases), while the capacity of the photovoltaic system increases much less. The reduction in grid electricity consumption is therefore lower in Brussels than in Pisa (maximum -11 % compared with -22 %). The gain in annualised energy cost is also logically much lower (maximum -2.6 % compared with -7.1 %). It can therefore be seen that benefiting from a non-zero feed-in tariff is less advantageous in Brussels, essentially because solar irradiance is lower there.

In terms of dynamic retail tariff, the analysis shows that photovoltaic capacity is much more reduced in Brussels than in Pisa. This can be explained by the lower irradiance during periods of high energy demand (autumn and winter), but also by the fact that the price of electricity is lower when the system produces the most, which reduces its profitability. It should also be noted that storage capacity increases significantly with the level of fluctuation, so as to gain resilience and face price rises during morning and evening peaks.

Generally speaking, this analysis on the case of Brussels illustrates that the higher the heating demand during the cold season, and the lower the solar irradiance and the less evenly distributed it is over the year, the less interesting the Carnot battery. Conversely, when heating demand is lower and irradiance better distributed, having a heat engine to carry out electrical discharges during the warm season is a real advantage.

4. Discussions and perspectives

The results obtained in Section 3 were used to answer the main research questions of this work. It was shown that, for most of the investment costs considered, installing a Carnot battery was a preferable option for minimising the energy system costs. The optimal operation of each component has also been characterised. In addition to these conclusions, the results raise new questions and offer new perspectives. These are detailed below.

Firstly, the study carried out here assumed an electricity price of 0.30 €/kWh. However, since electricity prices vary by region and over time, it is essential to generalise these findings.

A potential approach could be to express each investment cost as function of the electricity price. This would allow the CAPEX/p_{elec} ratio to be used to generalise the optimal design of the energy system. While the results in Section 3 are expressed in terms of CAPEX for the sake of readability and ease of interpretation, further investigation is necessary to ensure the CAPEX/p_{elec} ratio can faithfully depict the correct results trends.

With regard to heat production, the sensitivity analysis in Section 3.4 clearly demonstrated that the COP of the heat pump was a key parameter to reduce the annualised energy cost. In order to maximise the COP, technological improvements can obviously be expected. In addition to this, it also seems appropriate to reduce the temperature of the heat produced during the cold season, when there is no electrical discharge. Decreasing this temperature closer to that of the district heating network (i.e. 70°C) would increase the COP, and therefore reduce electricity consumption (essentially absorbed from the grid). However, for a given volume of the storage tanks, this would reduce storage capacity. For instance, going from 95°C/65°C to 80°C/65°C would roughly halve the storage capacity. As a result, more electricity imports would be required, which would partially offset the gain from the increased COP. Another option would be to maintain this storage capacity by increasing the tanks volume, and to consider the financial impact on the investment cost. A final option would be to distinguish between production modes: lower temperature when coupled directly to the heating network, and higher temperature when charging the thermal storage.

The sensitivity analysis also suggests that, given the impact of the COP, neglecting performance degradation at part load and the energy consumption associated with cold start-ups and transients is a very optimistic assumption. If these efficiency degradations were taken into account in our model, the impact would be, on the one hand, an increase in electricity consumption. On the other hand, a probable downsizing of the heat pump, so as to increase the average capacity factor and reduce part load operations, and to limit the number of start-ups, while the capacity of the thermal energy storage would be increased. This would result in a better COP. To deal with part load efficiency degradation in practice, several smaller capacity heat pumps could be set up in parallel. After optimal dispatch, taking into account the part load performance degradation, the heat pumps would be switched on progressively to maximise the overall COP of the installation.

Given the share of heat in the cost of energy, reducing the thermal demand seems to be a key lever. This can be achieved by insulating the building (efficiency measure), and by reducing the set-point temperature (sufficiency measure). Consequently, studying a scenario with a reduced heat demand is a real stake. If the need for thermal storage during the cold season is reduced, it is likely that the storage capacity will also be reduced. As a result, the role of the heat engine would become uncertain. Would it still be used?

Another hypothesis that may be questioned is that of perfect annual foresight. Since the model knows the boundary conditions perfectly well at every hour of the year, it can optimally anticipate the system's operations. For example, if the model sees a week coming with high demand and low energy production, it can anticipate this the week before by increasing the storage charge level. Another example would be to take advantage of low electricity costs to anticipate a high-cost week. Although this would allow the system to be optimised as much as possible, it is not entirely realistic. Weather forecasts, which influence photovoltaic production and heat demand, are generally uncertain more than 24 hours ahead. The same applies to the electricity price, which is set 24 hours before delivery on the day-ahead market. However, the impact of this hypothesis should be moderated. As illustrated in the analysis of the system operations in Section 3.2, the thermal storage is designed for daily use. As the charge-discharge cycles do not take place over more than two days, the storage does not allow for weekly or seasonal optimisation. The assumption of perfect foresight is therefore reasonable in this case. However, it would be less acceptable if the storage cycles took place over a longer period.

The results obtained in this work also pave the way for the use of reversible heat pumps/organic Rankine cycle. As introduced by Dumont et al. [14] in domestic applications, and recently studied by Scharrer et al. [30] for residential Carnot batteries, these machines would make it possible to significantly reduce investment costs. The counterpart to this cost reduction would be a slight loss of performance. As illustrated above, such performance degradation would not be detrimental to the electricity production with the heat engine, but severely to the thermal production with the heat pump. This precisely indicates that when designing a reversible machine, priority should be given to optimising the heat pump and not the organic Rankine cycle. This deserves further investigation.

As far as thermal storage is concerned, the considered costs (i.e. 20 to 40 €/kWh) and self-discharge losses (i.e. 5 %/24 h) did not make it possible to obtain a design allowing long-term storage (weekly, or seasonal). However, given the very low costs reported for pit-storage projects (down to 0.5 €/kWh [55]), it would seem appropriate to consider this technology. Although it is compatible in terms of temperature ranges, a better characterisation of self-discharge losses would be necessary, as they directly affect the temperature levels. Up to 30 % of self-discharge losses are for instance reported for annual cycles [55]. In order to model them correctly, a dynamic consideration of the storage temperature would be a minimum requirement. It would then be interesting to study whether, at the housing development level, long-term storage takes place primarily for heat, or also for electricity.

To finish this section, it must be stressed that future work should also focus on a comparison with chemical batteries (Li-ion). On a domestic scale, this technology is the first direct competitor of the Carnot battery. With its constantly falling costs (-90 % in last 15 years [56]) and very high efficiency (> 90 %), it appears to have a clear techno-economic lead. However, these two technologies do not provide the same services to energy systems (storage duration, heat/electricity coupling, etc.). What is more, the environmental footprint of Carnot batteries could be smaller [9]. There is therefore a need to study the complementarity between these technologies in order to identify possible synergies leading to an economic and environmental optimum. This will be the subject of a future study by the authors.

5. Concluding remarks

This work looked at the techno-economic potential of Carnot batteries used as flexibility options for heat and power management in residential applications. The system studied consists of a high temperature air-source heat pump connected to a thermal storage. Thermal discharge takes place through a heat exchanger connected to the district heating network, while electrical discharge takes place through an air-cooled organic Rankine cycle. The system is integrated into a housing development of 20 dwellings, and two locations with different climates are considered (Pisa and Brussels). The entire system (i.e. design and operations) is optimised to minimise the annualised energy cost using quadratically constrained linear programming. The main conclusions of this work are as follows:

- Domestic Carnot batteries help to minimise the annualised energy cost. The amount of energy stored, and therefore the degree of energy self-sufficiency, will depend on the cost of each of the components. Pisa also performs better than Brussels, mainly because of the higher solar irradiance and lower heat demand.

- The role that the Carnot battery will play in the energy system will vary according to the season. During autumn and winter, when photovoltaic production is lowest and demand for heat is highest, only thermal discharge occurs. Storage acts as a buffer between peaks in heat demand and heat pump production.

  Conversely, in spring and summer, when photovoltaic production is at its peak and demand for heat is at its lowest, the heat accumulated in the storage during the day is used mainly to power the heat engine and produce electricity in the morning and evening. This result shows that despite the low electrical efficiency of the Carnot battery (less than 25 %), investing in a heat engine to be coupled to the thermal storage is financially preferable to curtailment.

- For fluctuation levels comparable to those encountered on the day-ahead markets today, benefiting from a dynamic retail tariff is not financially advantageous. Dynamic tariffs indeed lead to an average increase in electricity prices when demand is at its highest (autumn/winter and morning/evening peaks).

  For higher levels of fluctuation, the Carnot battery is a good option, as it allows energy arbitrage. It should be noted, however, that variable tariffs can cause reduction in the installed photovoltaic capacity, and therefore reduce the energy self-sufficiency.

- On the other hand, benefiting from a non-zero feed-in tariff is not really favourable to the Carnot battery, although it does allow a slight reduction in the annualised energy cost (generally less than 5 %). Indeed, the capacity of the heat engine is significantly reduced in Pisa and generally zero in Brussels.

From this work, we can conclude that if a heat pump and thermal storage are installed, then installing a heat engine is generally profitable, no matter how efficient it is, as long as its cost allows.

In order to increase profitability, future work on the subject could look into the use of different storage temperature levels depending on the season (colder when there is no electrical discharge). Also, the profitability of reversible heat pumps/heat engines should be investigated, because although they allow a reduction in investment costs, they are generally accompanied by a reduction in coefficient of performance and efficiency. Finally, the feasibility of this type of system should be confirmed with more accurate models, including operational models that take into account part load efficiency degradation, fluctuation of storage temperature, as well as a characterisation of dynamic performance.

Declaration of competing interest

The authors declare that they have no known competing financial interests or personal relationships that could have appeared to influence the work reported in this paper.

Acknowledgements

The first author acknowledges the support of Fonds de la Recherche Scientifique - FNRS [40021673 FRIA-B2].

Appendix A. Results for Brussels case study

In Brussels, the specific heating requirements are 93 kWh/m^2/year and the domestic hot water demand is 21 kWh/m^2/year. The electricity demand is 20 kWh/m^2/year. Finally, the specific cooling requirements are 14 kWh/m^2/year. Assuming that the air-cooled chillers have a Carnot efficiency of 45 %, the corresponding specific electricity consumption is 1.4 kWh/m^2/year. The corresponding time series are depicted in Fig. A.1. The optimum

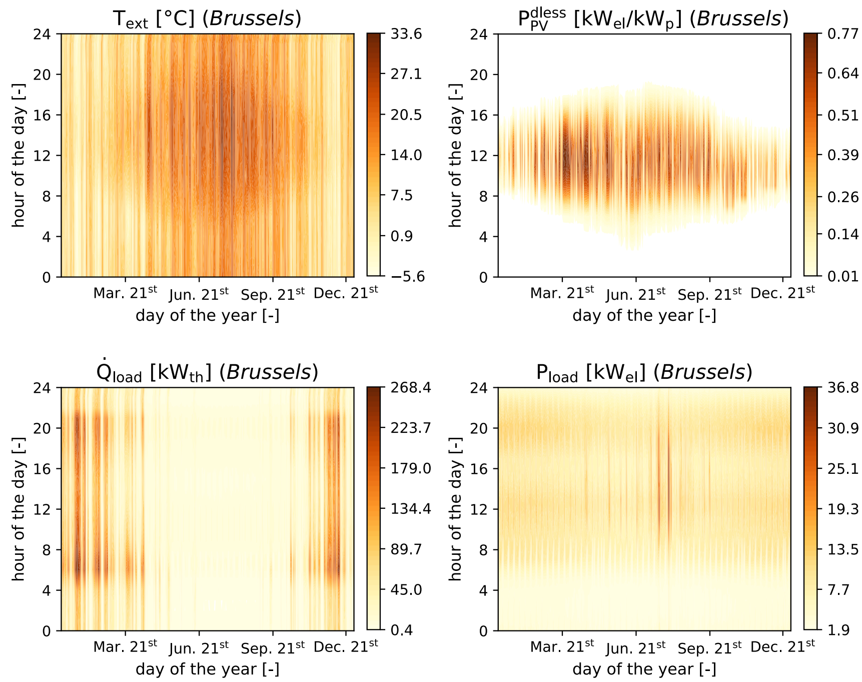

Figure A.1: Temporal heatmaps representing the climate and demand profiles for Brussels. The the days of the year are plotted along the x-axis, and hours of the day are plotted along the y-axis. P_{load} and $\dot{Q}_{load}$ are the total electrical and thermal loads. T_{ext} is the external temperature and P_{PV}^{dless} is the dimensionless photovoltaic production per installed capacity.

system designs and corresponding performance indicators are depicted in Fig. A.2. The operations corresponding to the case $CAPEX_{HP}$ = 600 €/kW_{th}, $CAPEX_{HE}$ = 2400 €/kW_{el} and $CAPEX_{TES}$ = 30 €/kWh_{th} are depicted in Fig. A.3. The seasonal indicators corresponding to the case $CAPEX_{HP}$ = 600 €/kW_{th}, $CAPEX_{HE}$ = 2400 €/kW_{el} and $CAPEX_{TES}$ = 30 €/kWh_{th} are given in Table A.1. The optimum design corresponding to the case $CAPEX_{HP}$ = 600 €/kW_{th}, $CAPEX_{HE}$ = 2400 €/kW_{el} and $CAPEX_{TES}$ = 30 €/kWh_{th} is given in Table A.2. The relative deviations in optimum system designs and corresponding performance indicators due to non-zero feed-in tariff are depicted in Fig. A.4. Fig. A.5 depicts the relative deviation in annualised energy cost, photovoltaic, thermal energy storage and heat engine capacities for coefficients of variation from 0 % to 100 %. Finally, Fig. A.6

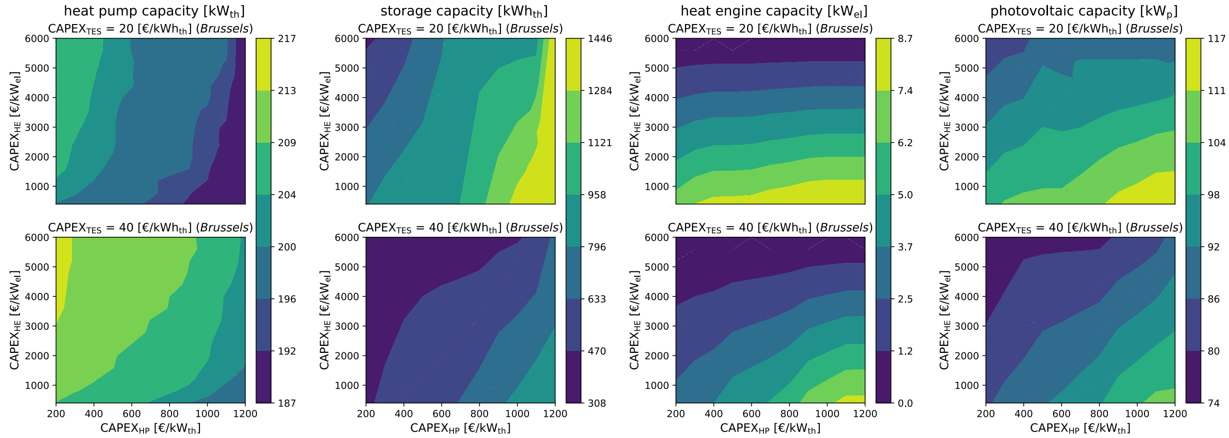

(a) Installed heat pump capacity.

(b) Installed thermal storage capacity

(c) Installed heat engine capacity.

(d) Installed photovoltaic capacity.

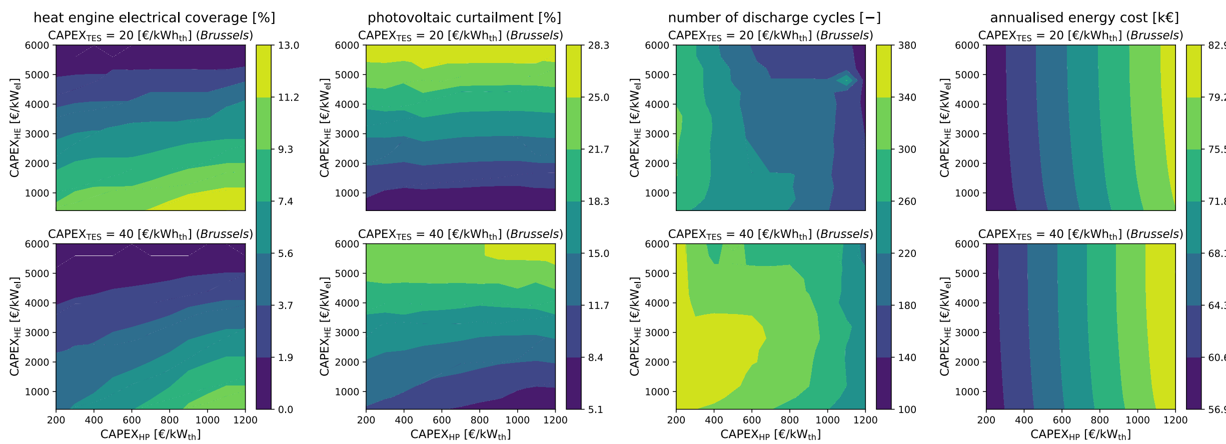

(e) Fraction of electricity consumption covered by the heat engine.

(f) Fraction of curtailed photovoltaic production.

(g) Number of discharge cycles for the storage.

(h) Annualised energy cost.

Figure A.2: Optimum system design and performance indicators for the system operations based on the investment costs considered. The colourmaps depict the installed capacities. The x-axis represents the costs considered for the heat pump, the y-axis the costs of the heat engine and the top and bottom maps illustrate two different storage costs.

depicts the Sobol indices for each uncertain parameter.

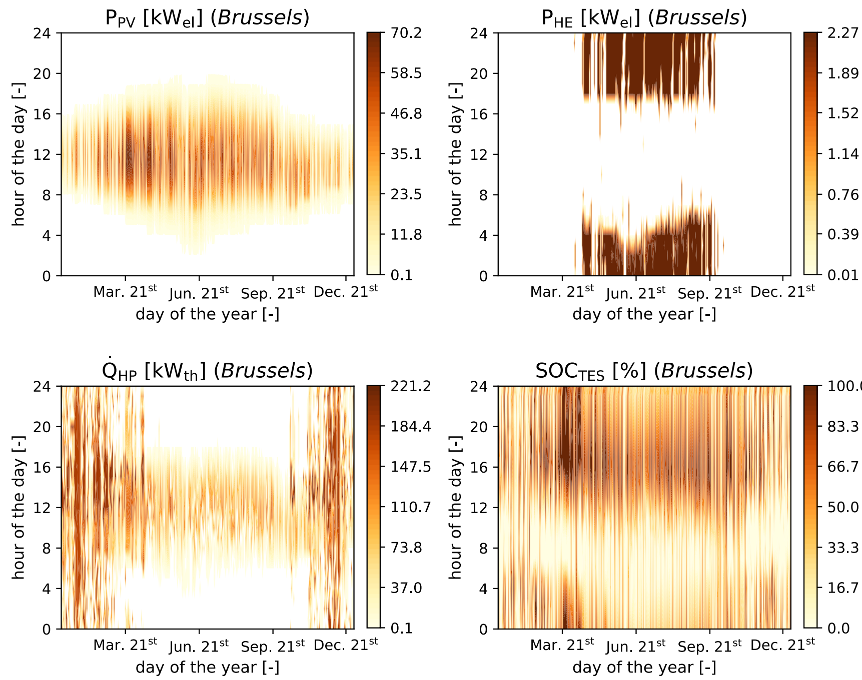

Figure A.3: Temporal heatmaps representing the system operations for Brussels (photovoltaic power production P_{PV}, heat engine power production P_{HE}, heat pump thermal production $\dot{Q}_{HP}$ and storage state-of-charge SOC_{TES}). The the days of the year are plotted along the x-axis, and hours of the day are plotted along the y-axis.

Appendix B. Analysis of representative days

This appendix illustrates the operations of the energy system for two representative days out of the 365 simulated: Fig. B.1 shows a typical summer day and Fig. B.2 shows a typical winter day. In Fig. B.1, the Carnot battery's role in shifting photovoltaic production is clearly visible: the storage is charged by the heat pump during hours of production, while it is discharged by the heat engine when the sun is not shining. During the morning hours, the heat engine is sufficient to cover the electric load, while the grid is used as a backup to face the evening peak. Curtailment also occurs due to excess electricity generation.

In Fig. B.2, the buffer role of thermal storage is perfectly illustrated. It allows the heat pump to operate close to full load throughout the day, while the storage charges (resp. discharges) when production exceeds (resp. does not meet) the thermal load. In addition,

Table A.1: Seasonal operations and performance indicators for Brussels. The considered design is for $CAPEX_{HP}$ = 600 €/kW_{th}, $CAPEX_{HE}$ = 2400 €/kW_{el} and $CAPEX_{TES}$ = 30 €/kWh_{th}. Astronomical seasons are here considered. During winter, the slight difference between heat production and demand is due to the thermal losses in the storage. N_{cycles} is the number of charging/discharging cycles of the thermal storage and E^{abs}_{grid} is the grid electricity consumption.

Parameter	**Unit**	**Winter**	**Spring**	**Summer**	**Autumn**	**Annual**
E^{th}_{load}	MWh_{th}	160.2	55.1	16.8	109.9	342.0
E_{HP}	MWh_{th}	161.1	72.2	45.8	112.3	391.4
COP_{HP}	-	2.41	2.70	3.14	2.46	2.54
E^{el}_{load}	MWh_{el}	17.2	14.5	16.2	16.3	64.2
E_{HE}	MWh_{el}	0.00	1.29	2.17	0.14	3.60
η_{HE}	%	n.a.	8.18	7.83	8.00	7.96
$COP_{HP} \cdot \eta_{HE}$	%	n.a.	22.1	24.6	19.7	20.2
N_{cycles}	-	88.2	71.2	64.6	71.0	295.0
E_{PV}	MWh_{el}	13.3	33.4	30.9	13.3	90.9
E^{abs}_{grid}	MWh_{el}	70.9	11.6	4.0	48.6	135.1

Table A.2: Nominal system design for Brussels for $CAPEX_{HP}$ = 600 €/kW_{th}, $CAPEX_{HE}$ = 2400 €/kW_{el} and $CAPEX_{TES}$ = 30 €/kWh_{th}.

Parameter	**Symbol**	**Value**	**Unit**
Heat pump capacity	$\dot{Q}^{nom}_{HP}$	205.1	kW_{th}
Storage capacity	E^{nom}_{TES}	588	kWh_{th}
Total storage volume	V^{nom}_{TES}	34.6	m^3
Heat engine capacity	P^{nom}_{HE}	2.27	kW_{el}
Photovoltaic capacity	P^{nom}_{PV}	91.6	kW_p
Annualised energy cost	AEC	67.8	k€

since photovoltaic production is not sufficient, the grid is used throughout the entire day. The heat engine is therefore not used.

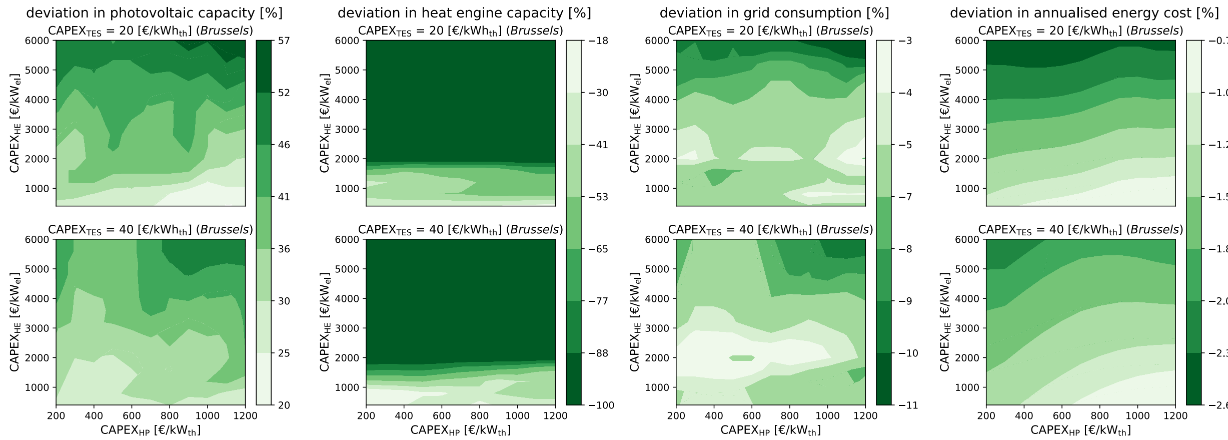

(a) Photovoltaic capacity. (b) Heat engine capacity. (c) Grid electricity consumption. (d) Annualised energy cost.

Figure A.4: Deviations in installed capacities and performance indicators due to non-zero feed-in tariff. The colourmaps depict the relative deviations. The x-axis represents the costs considered for the heat pump, the y-axis the costs of the heat engine and the top and bottom maps illustrate two different storage costs.

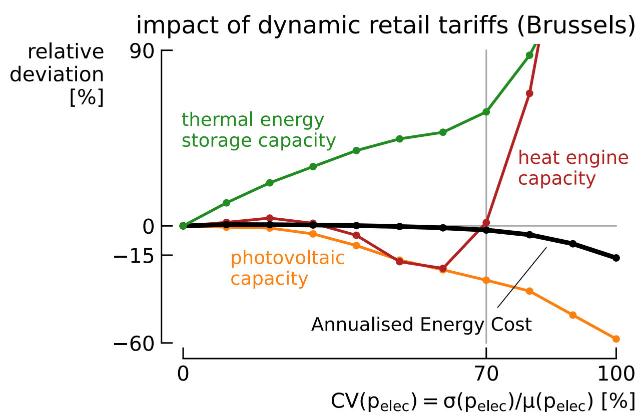

Figure A.5: Relative deviation in annualised energy cost, photovoltaic, storage and heat engine capacities for different coefficients of variation of retail tariffs. The design corresponding to case $\text{CAPEX}_{\text{HP}} = 600$ €/kW$_{\text{th}}$, $\text{CAPEX}_{\text{HE}} = 2400$ €/kW$_{\text{el}}$ and $\text{CAPEX}_{\text{TES}} = 30$ €/kWh$_{\text{th}}$ was selected for the analysis.

References

[1] Q. Chen, Z. Kuang, X. Liu, T. Zhang, Energy storage to solve the diurnal, weekly, and seasonal mismatch and achieve zero-carbon electricity consumption in buildings, Applied Energy 312 (2022) 118744. doi:10.1016/j.apenergy.2022.118744.

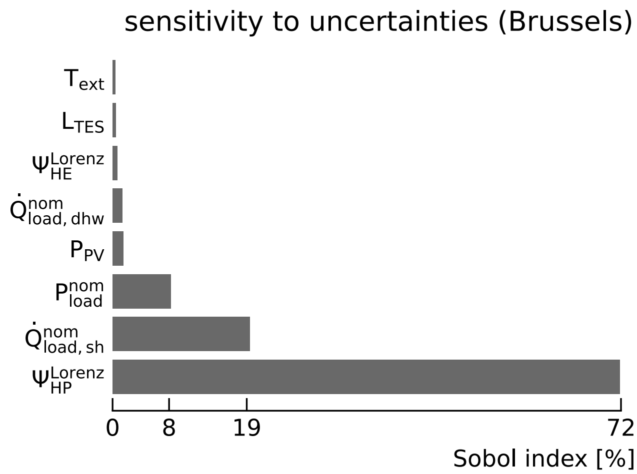

Figure A.6: Sobol indices corresponding to the uncertain parameters considered in the sensitivity analysis (Table 4). The design corresponding to case $CAPEX_{HP}$ = 600 €/kW_{th}, $CAPEX_{HE}$ = 2400 €/kW_{el} and $CAPEX_{TES}$ = 30 €/kWh_{th} was selected for the analysis.

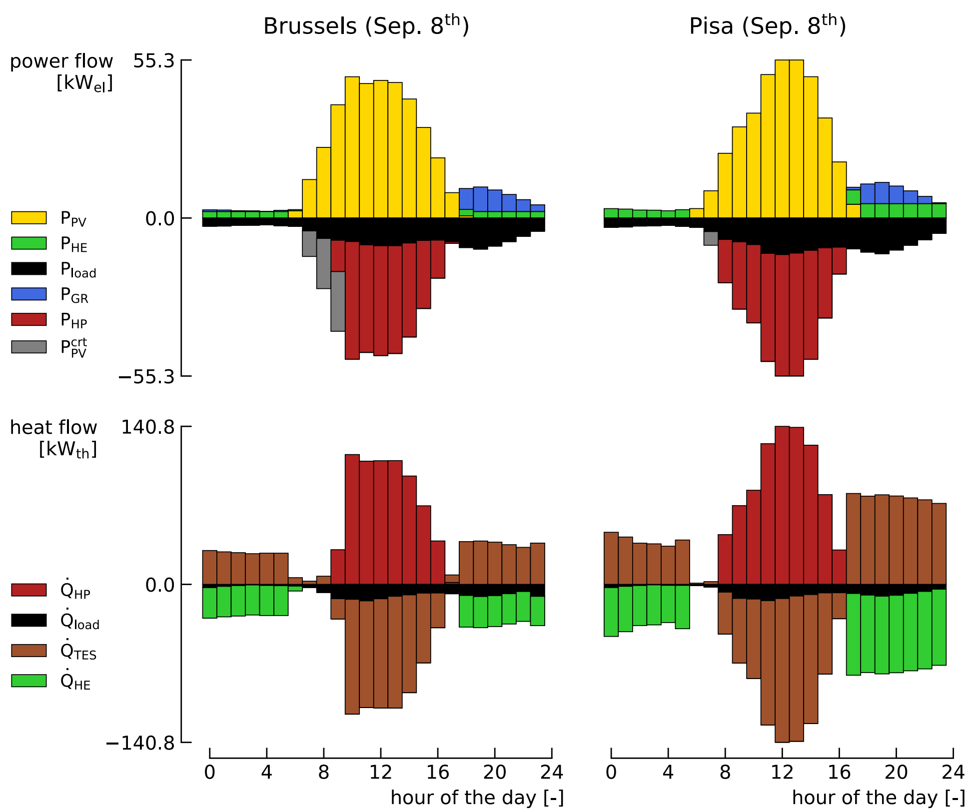

Figure B.1: System operations for a representative summer day.

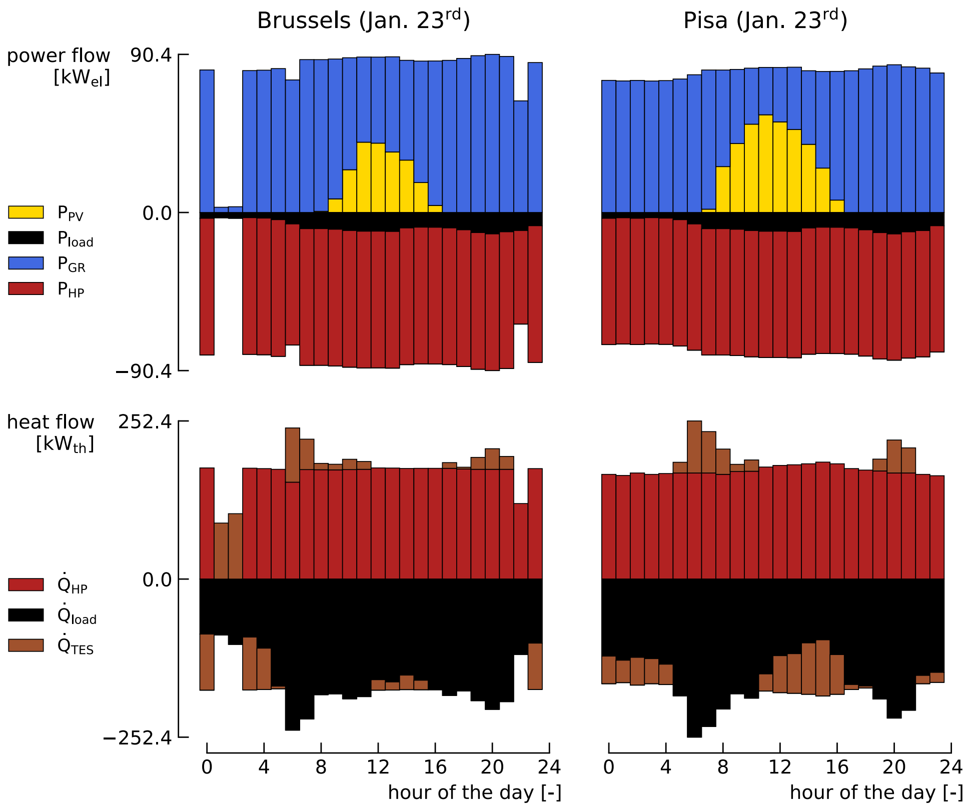

Figure B.2: System operations for a representative winter day.

URL https://www.sciencedirect.com/science/article/pii/S0306261922002008

[2] G. De Carne, G. Buticchi, Z. Zou, M. Liserre, Reverse Power Flow Control in a ST-Fed Distribution Grid, IEEE Transactions on Smart Grid 9 (4) (2018) 3811–3819, conference Name: IEEE Transactions on Smart Grid. doi:10.1109/TSG.2017.2651147.
URL https://ieeexplore.ieee.org/document/7812791

[3] R. Luthander, D. Lingfors, J. Widén, Large-scale integration of photovoltaic power in a distribution grid using power curtailment and energy storage, Solar Energy 155 (2017) 1319–1325. doi:10.1016/j.solener.2017.07.083.
URL https://www.sciencedirect.com/science/article/pii/S0038092X17306680

[4] L. Langer, T. Volling, An optimal home energy management system for modulating heat pumps and photovoltaic systems, Applied Energy 278 (2020) 115661. doi:

10.1016/j.apenergy.2020.115661.
URL https://www.sciencedirect.com/science/article/pii/S0306261920311570

[5] A. Arteconi, N. Hewitt, F. Polonara, Domestic demand-side management (DSM): Role of heat pumps and thermal energy storage (TES) systems, Applied Thermal Engineering 51 (1-2) (2013) 155–165. doi:10.1016/j.applthermaleng.2012.09.023.
URL https://linkinghub.elsevier.com/retrieve/pii/S1359431112006357

[6] D. Coppitters, W. De Paepe, F. Contino, Robust design optimization of a photovoltaic-battery-heat pump system with thermal storage under aleatory and epistemic uncertainty, Energy 229 (2021) 120692. doi:10.1016/j.energy.2021.120692.
URL https://linkinghub.elsevier.com/retrieve/pii/S0360544221009403

[7] A. Pena-Bello, P. Schuetz, M. Berger, J. Worlitschek, M. K. Patel, D. Parra, Decarbonizing heat with PV-coupled heat pumps supported by electricity and heat storage: Impacts and trade-offs for prosumers and the grid, Energy Conversion and Management 240 (2021) 114220. doi:10.1016/j.enconman.2021.114220.
URL https://www.sciencedirect.com/science/article/pii/S0196890421003964

[8] W.-D. Steinmann, D. Bauer, H. Jockenhöfer, M. Johnson, Pumped thermal energy storage (PTES) as smart sector-coupling technology for heat and electricity, Energy 183 (2019) 185–190. doi:10.1016/j.energy.2019.06.058.
URL https://linkinghub.elsevier.com/retrieve/pii/S0360544219311879

[9] G. F. Frate, L. Ferrari, P. Sdringola, U. Desideri, A. Sciacovelli, Thermally integrated pumped thermal energy storage for multi-energy districts: Integrated modelling, assessment and comparison with batteries, Journal of Energy Storage 61 (2023) 106734. doi:10.1016/j.est.2023.106734.
URL https://www.sciencedirect.com/science/article/pii/S2352152X23001317

[10] O. Dumont, G. F. Frate, A. Pillai, S. Lecompte, M. De Paepe, V. Lemort, Carnot

battery technology: A state-of-the-art review, Journal of Energy Storage 32 (Sep. 2020). doi:10.1016/j.est.2020.101756.

[11] A. Datas, A. Ramos, C. del Cañizo, Techno-economic analysis of solar PV power-to-heat-to-power storage and trigeneration in the residential sector, Applied Energy 256 (2019) 113935. doi:10.1016/j.apenergy.2019.113935.
URL https://www.sciencedirect.com/science/article/pii/S0306261919316228

[12] G. F. Frate, L. Ferrari, U. Desideri, Rankine Carnot Batteries with the Integration of Thermal Energy Sources: A Review, Energies 13 (18) (2020) 4766, number: 18 Publisher: Multidisciplinary Digital Publishing Institute. doi:10.3390/en13184766.
URL https://www.mdpi.com/1996-1073/13/18/4766

[13] A. Olympios, J. McTigue, P. Farres-Antunez, A. Tafone, A. Romagnoli, Y. Li, Y. Ding, W.-D. Steinmann, L. Wang, H. Chen, C. Markides, Progress and prospects of thermo-mechanical energy storage - A critical review, Progress in Energy (Jan. 2021). doi:10.1088/2516-1083/abdbba.

[14] O. Dumont, S. Quoilin, V. Lemort, Experimental investigation of a reversible heat pump/organic Rankine cycle unit designed to be coupled with a passive house to get a Net Zero Energy Building, International Journal of Refrigeration 54 (2015) 190–203. doi:10.1016/j.ijrefrig.2015.03.008.
URL https://linkinghub.elsevier.com/retrieve/pii/S0140700715000638

[15] S. Staub, P. Bazan, K. Braimakis, D. Müller, C. Regensburger, D. Scharrer, B. Schmitt, D. Steger, R. German, S. Karellas, M. Pruckner, E. Schlücker, S. Will, J. Karl, Reversible Heat Pump–Organic Rankine Cycle Systems for the Storage of Renewable Electricity, Energies 11 (6) (2018) 1352, number: 6 Publisher: Multidisciplinary Digital Publishing Institute. doi:10.3390/en11061352.
URL https://www.mdpi.com/1996-1073/11/6/1352

[16] B. Eppinger, D. Steger, C. Regensburger, J. Karl, E. Schlücker, S. Will, Carnot battery:

Simulation and design of a reversible heat pump-organic Rankine cycle pilot plant, Applied Energy 288 (2021) 116650. doi:10.1016/j.apenergy.2021.116650.
URL https://linkinghub.elsevier.com/retrieve/pii/S0306261921001835

[17] M. Weitzer, D. Müller, J. Karl, Two-phase expansion processes in heat pump – ORC systems (Carnot batteries) with volumetric machines for enhanced off-design efficiency, Renewable Energy 199 (2022) 720–732. doi:10.1016/j.renene.2022.08.143.
URL https://www.sciencedirect.com/science/article/pii/S0960148122013222

[18] G. F. Frate, L. Ferrari, U. Desideri, Multi-Criteria Economic Analysis of a Pumped Thermal Electricity Storage (PTES) With Thermal Integration, Frontiers in Energy Research 8 (2020) 53. doi:10.3389/fenrg.2020.00053.
URL https://www.frontiersin.org/article/10.3389/fenrg.2020.00053/full

[19] S. Hu, Z. Yang, J. Li, Y. Duan, Thermo-economic analysis of the pumped thermal energy storage with thermal integration in different application scenarios, Energy Conversion and Management 236 (2021) 114072. doi:10.1016/j.enconman.2021.114072.
URL https://linkinghub.elsevier.com/retrieve/pii/S019689042100248X

[20] J. D. McTigue, P. Farres-Antunez, K. S. J, C. N. Markides, A. J. White, Techno-economic analysis of recuperated Joule-Brayton pumped thermal energy storage, Energy Conversion and Management 252 (2022) 115016. doi:10.1016/j.enconman.2021.115016.
URL https://www.sciencedirect.com/science/article/pii/S0196890421011924

[21] P. Sorknæs, J. Z. Thellufsen, K. Knobloch, K. Engelbrecht, M. Yuan, Economic potentials of carnot batteries in 100% renewable energy systems, Energy 282 (2023) 128837. doi:10.1016/j.energy.2023.128837.
URL https://www.sciencedirect.com/science/article/pii/S0360544223022314

[22] F. Nitsch, M. Wetzel, H. C. Gils, K. Nienhaus, The future role of Carnot batteries in Central Europe: Combining energy system and market perspective, Journal of Energy

Storage 85 (2024) 110959. doi:10.1016/j.est.2024.110959.
URL https://www.sciencedirect.com/science/article/pii/S2352152X24005437

[23] R. Fan, H. Xi, Energy, exergy, economic (3E) analysis, optimization and comparison of different Carnot battery systems for energy storage, Energy Conversion and Management 252 (2022) 115037. doi:10.1016/j.enconman.2021.115037.
URL https://www.sciencedirect.com/science/article/pii/S0196890421012139

[24] R. Fan, H. Xi, Exergoeconomic optimization and working fluid comparison of low-temperature Carnot battery systems for energy storage, Journal of Energy Storage 51 (2022) 104453. doi:10.1016/j.est.2022.104453.
URL https://www.sciencedirect.com/science/article/pii/S2352152X22004753

[25] Y. Zhang, L. Xu, J. Li, L. Zhang, Z. Yuan, Technical and economic evaluation, comparison and optimization of a Carnot battery with two different layouts, Journal of Energy Storage 55 (2022) 105583. doi:10.1016/j.est.2022.105583.
URL https://www.sciencedirect.com/science/article/pii/S2352152X22015717

[26] J. Niu, J. Wang, X. Liu, L. Dong, Optimal integration of solar collectors to Carnot battery system with regenerators, Energy Conversion and Management 277 (2023) 116625. doi:10.1016/j.enconman.2022.116625.
URL https://www.sciencedirect.com/science/article/pii/S0196890422014030

[27] X. Yu, H. Qiao, B. Yang, H. Zhang, Thermal-economic and sensitivity analysis of different Rankine-based Carnot battery configurations for energy storage, Energy Conversion and Management 283 (2023) 116959. doi:10.1016/j.enconman.2023.116959.
URL https://www.sciencedirect.com/science/article/pii/S0196890423003059

[28] Z. Su, L. Yang, J. Song, X. Jin, X. Wu, X. Li, Multi-dimensional comparison and multi-objective optimization of geothermal-assisted Carnot battery for photovoltaic load shifting, Energy Conversion and Management 289 (2023) 117156. doi:

10.1016/j.enconman.2023.117156.
URL https://www.sciencedirect.com/science/article/pii/S0196890423005022

[29] R. Tassenoy, K. Couvreur, W. Beyne, M. De Paepe, S. Lecompte, Techno-economic assessment of Carnot batteries for load-shifting of solar PV production of an office building, Renewable Energy 199 (2022) 1133–1144. doi:10.1016/j.renene.2022.09.039.
URL https://www.sciencedirect.com/science/article/pii/S0960148122013891

[30] D. Scharrer, P. Bazan, M. Pruckner, R. German, Simulation and analysis of a Carnot Battery consisting of a reversible heat pump/organic Rankine cycle for a domestic application in a community with varying number of houses, Energy 261 (2022) 125166. doi:10.1016/j.energy.2022.125166.
URL https://www.sciencedirect.com/science/article/pii/S0360544222020588

[31] C. Poletto, O. Dumont, A. De Pascale, V. Lemort, S. Ottaviano, O. Thomé, Control strategy and performance of a small-size thermally integrated Carnot battery based on a Rankine cycle and combined with district heating, Energy Conversion and Management 302 (2024) 118111. doi:10.1016/j.enconman.2024.118111.
URL https://www.sciencedirect.com/science/article/pii/S0196890424000529

[32] A. Laterre, O. Dumont, V. Lemort, F. Contino, Is waste heat recovery a promising avenue for the Carnot battery? Techno-economic optimisation of an electric booster-assisted Carnot battery integrated into different data centres, Energy Conversion and Management 301 (2024) 118030. doi:10.1016/j.enconman.2023.118030.
URL https://www.sciencedirect.com/science/article/pii/S0196890423013766

[33] O. Dumont, V. Lemort, Mapping of performance of pumped thermal energy storage (Carnot battery) using waste heat recovery, Energy 211 (2020) 118963. doi:10.1016/j.energy.2020.118963.
URL https://linkinghub.elsevier.com/retrieve/pii/S0360544220320703

[34] M. Weitzer, D. Müller, D. Steger, A. Charalampidis, S. Karellas, J. Karl, Or-

ganic flash cycles in Rankine-based Carnot batteries with large storage temperature spreads, Energy Conversion and Management 255 (2022) 115323. doi:10.1016/j.enconman.2022.115323.
URL https://www.sciencedirect.com/science/article/pii/S0196890422001194

[35] M. Wirtz, nPro: A web-based planning tool for designing district energy systems and thermal networks, Energy 268 (2023) 126575. doi:10.1016/j.energy.2022.126575.
URL https://www.sciencedirect.com/science/article/pii/S0360544222034624

[36] G. Limpens, S. Moret, H. Jeanmart, F. Maréchal, EnergyScope TD: A novel open-source model for regional energy systems, Applied Energy 255 (2019) 113729. doi:10.1016/j.apenergy.2019.113729.
URL https://www.sciencedirect.com/science/article/pii/S0306261919314163

[37] D. E. Agency, Technology Data for Generation of Electricity and District Heating, Tech. rep., Danish Energy Agency (Feb. 2023).

[38] B. Zühlsdorf, J. L. Poulsen, S. Dusek, V. Wilk, J. Krämer, R. Rieberer, M. Verdnik, T. Demeester, E. Vieren, C. Magni, H. Abedini, C. Leroy, L. Yang, M. P. Andersen, B. Elmegaard, T. Turunen-Saaresti, A. Uusitalo, F. De Carlan, C. Gachot, F. Schlosser, S. Klöppel, O. Abu Khass, R. Schaffrath, U. Wittstadt, S. Henninger, H. Teles de Oliveira, T. Kaida, M. Ramirez, J.-A. Lycklama a Nijeholt, C. Schlemminger, O. Marius Moen, G. Lee, C. Arpagaus, High-Temperature Heat Pumps. Task 1 – Technologies.: Task Report, Report, IEA Heat Pump Centre, publication Title: High-Temperature Heat Pumps. Task 1 – Technologies. (2023).

[39] S. Lemmens, Cost Engineering Techniques and Their Applicability for Cost Estimation of Organic Rankine Cycle Systems, Energies 9 (7) (2016) 485. doi:10.3390/en9070485.
URL http://www.mdpi.com/1996-1073/9/7/485

[40] L. Tocci, T. Pal, I. Pesmazoglou, B. Franchetti, Small Scale Organic Rankine Cycle (ORC): A Techno-Economic Review, Energies 10 (4) (2017) 413, number: 4 Publisher:

Multidisciplinary Digital Publishing Institute. doi:10.3390/en10040413.
URL https://www.mdpi.com/1996-1073/10/4/413

[41] Eurostat, Electricity prices by type of user (Apr. 2024).
URL https://doi.org/10.2908/TEN00117

[42] L. Hirth, J. Mühlenpfordt, M. Bulkeley, The ENTSO-E Transparency Platform – A review of Europe's most ambitious electricity data platform, Applied Energy 225 (2018) 1054–1067. doi:10.1016/j.apenergy.2018.04.048.
URL https://www.sciencedirect.com/science/article/pii/S0306261918306068

[43] M. L. Bynum, G. A. Hackebeil, W. E. Hart, C. D. Laird, B. L. Nicholson, J. D. Siirola, J.-P. Watson, D. L. Woodruff, Pyomo — Optimization Modeling in Python, Vol. 67 of Springer Optimization and Its Applications, Springer International Publishing, Cham, 2021. doi:10.1007/978-3-030-68928-5.
URL http://link.springer.com/10.1007/978-3-030-68928-5

[44] L. Gurobi Optimization, Gurobi Optimizer Reference Manual (2023).
URL https://www.gurobi.com

[45] C. Arpagaus, F. Bless, M. Uhlmann, J. Schiffmann, S. S. Bertsch, High temperature heat pumps: Market overview, state of the art, research status, refrigerants, and application potentials, Energy 152 (2018) 985–1010. doi:10.1016/j.energy.2018.03.166.
URL https://www.sciencedirect.com/science/article/pii/S0360544218305759

[46] F. Schlosser, M. Jesper, J. Vogelsang, T. G. Walmsley, C. Arpagaus, J. Hesselbach, Large-scale heat pumps: Applications, performance, economic feasibility and industrial integration, Renewable and Sustainable Energy Reviews 133 (2020) 110219. doi:10.1016/j.rser.2020.110219.
URL https://www.sciencedirect.com/science/article/pii/S1364032120305086

[47] M. Pitarch, E. Hervas-Blasco, E. Navarro-Peris, J. Gonzálvez-Maciá, J. M. Corberán, Evaluation of optimal subcooling in subcritical heat pump systems, International Jour-

nal of Refrigeration 78 (2017) 18–31. doi:10.1016/j.ijrefrig.2017.03.015.
URL https://www.sciencedirect.com/science/article/pii/S014070071730110X

[48] H. Pieper, T. Ommen, F. Buhler, B. L. Paaske, B. Elmegaard, W. B. Markussen, Allocation of investment costs for large-scale heat pumps supplying district heating, Energy Procedia 147 (2018) 358–367. doi:10.1016/j.egypro.2018.07.104.
URL https://www.sciencedirect.com/science/article/pii/S1876610218302613

[49] J. K. Jensen, T. Ommen, L. Reinholdt, W. B. Markussen, B. Elmegaard, Heat pump COP, part 2: Generalized COP estimation of heat pump processes, Proceedings of the13th IIR-Gustav Lorentzen Conference on Natural Refrigerants 2 (2018) 1136–1145, publisher: International Institute of Refrigeration. doi:10.18462/iir.gl.2018.1386.

[50] H. Pieper, T. Ommen, J. Kjær Jensen, B. Elmegaard, W. Brix Markussen, Comparison of COP estimation methods for large-scale heat pumps used in energy planning, Energy 205 (2020) 117994. doi:10.1016/j.energy.2020.117994.
URL https://www.sciencedirect.com/science/article/pii/S0360544220311014

[51] H. Öhman, P. Lundqvist, Comparison and analysis of performance using Low Temperature Power Cycles, Applied Thermal Engineering 52 (1) (2013) 160–169. doi:10.1016/j.applthermaleng.2012.11.024.
URL https://www.sciencedirect.com/science/article/pii/S1359431112007375

[52] D. Coppitters, P. Tsirikoglou, W. D. Paepe, K. Kyprianidis, A. Kalfas, F. Contino, RHEIA: Robust design optimization of renewable Hydrogen and dErIved energy cArrier systems, Journal of Open Source Software 7 (75) (2022) 4370. doi:10.21105/joss.04370.
URL https://joss.theoj.org/papers/10.21105/joss.04370

[53] T. Kaschub, P. Jochem, W. Fichtner, Solar energy storage in German households: profitability, load changes and flexibility, Energy Policy 98 (2016) 520–532. doi:

10.1016/j.enpol.2016.09.017.
URL https://www.sciencedirect.com/science/article/pii/S0301421516304815

[54] B. Zakeri, S. Cross, P. E. Dodds, G. C. Gissey, Policy options for enhancing economic profitability of residential solar photovoltaic with battery energy storage, Applied Energy 290 (2021) 116697. doi:10.1016/j.apenergy.2021.116697.
URL https://www.sciencedirect.com/science/article/pii/S0306261921002221

[55] D. E. Agency, Technology Data for Energy Storage, Tech. rep., Danish Energy Agency (Jan. 2020).

[56] IEA, Batteries and Secure Energy Transitions, Tech. rep., IEA, Paris (2024).
URL https://www.iea.org/reports/batteries-and-secure-energy-transitions